

Self-discharge of Rechargeable Hybrid Aqueous Battery

by

Aishuak Konarov

A thesis

presented to the University of Waterloo

in fulfillment of the

thesis requirement for the degree of

Master of Applied Science

in

Chemical Engineering

Waterloo, Ontario, Canada, 2014

©Aishuak Konarov 2014

AUTHOR'S DECLARATION

I hereby declare that I am the sole author of this thesis. This is a true copy of the thesis, including any required final revisions, as accepted by my examiners.

I understand that my thesis may be made electronically available to the public.

Abstract

This thesis studies the self-discharge performance of recently developed rechargeable hybrid aqueous batteries, using LiMn_2O_4 as a cathode and Zinc as an anode. It is shown through a variety of electrochemical and *ex-situ* analytical techniques that many parts of the composite cathode play important roles on the self-discharge of the battery. It was determined that the current collector must be passive towards corrosion, and polyethylene was identified as the best option for this application. The effect of amount and type of conductive agent was also investigated, with low surface area carbonaceous material giving best performances. It was also shown that the state of charge has strong effects on the extension of self-discharge. More importantly, this study shows that the self-discharge mechanism in the ReHAB system involves the cathode active material and contains a reversible and an irreversible part. The reversible portion is predominant and is due to lithium re-intercalation into the LiMn_2O_4 spinel framework, and results from Zn dissolution into the electrolyte, which drives the Li^+ ions out of the solution. The irreversible portion of the self-discharge occurs as a result of the decomposition of the LiMn_2O_4 material in the presence of the acidic electrolyte, and is much less extensive than the reversible process.

Acknowledgements

First of all, I would give my thanks to Allah for giving me strength and wisdom to achieve one of my goals. I wish to thank my mom and family for their limitless support and love.

I would like to give my sincere thanks to my supervisor Dr. Pu Chen for giving me the opportunity to do research in his group, which I was fortunate to be a part of, and for continuing to encourage me throughout my studies.

My special thanks to Dr. Zhumabay Bakenov for giving me the confidence to start on and continue on this master's journey, and always pointing me in the right direction. I am thankful to Dr. Denise Gosselink for teaching me how to do the research and write papers, also for taking the time to edit my manuscript, your input was invaluable.

I want to express my deepest gratitude to Dr. The Nam Long Doan, Dr. Yonguang Zhang for instructing how to assemble batteries and giving me useful advice and guidance. Next, I thank Ms Yan Zhao for her immediate support and help.

Additionally, I would like to thank former and current colleagues, Jing (Jim) Li, Kai (Allen) Li, Ji (Terry) Yan, Xianwen Wu, Qiang (Jason) Wang, Jeyeol Hwangbo Ye Tian, Yan (Ryan) Yu, Diana Askhatova, Kyung Eun Kate Sun for cooperation and inspirational conversations.

Dedication

Dedicated to my Family

Table of Contents

| | |
|---|------|
| AUTHOR'S DECLARATION | ii |
| Abstract | iii |
| Acknowledgements | iv |
| Dedication | iv |
| Table of Contents | vi |
| List of Figures | ix |
| List of Abbreviations | xiii |
| Chapter 1 Introduction | 1 |
| Chapter 2 Literature Review | 4 |
| 2.1 Li-ion Batteries | 4 |
| 2.2 Working Principle of Li-ion Batteries | 6 |
| 2.2.1 Cathode Materials for Li-ion Battery | 8 |
| 2.3 Aqueous Rechargeable Lithium Batteries | 12 |
| 2.3.1 Rechargeable Hybrid Aqueous Battery | 16 |
| 2.4 Self-discharge process | 19 |
| 2.4.1 Self-discharge in Li-ion Batteries | 20 |
| 2.4.2 Self-discharge in Lead-acid batteries | 23 |

| | |
|---|----|
| 2.4.3 Self-discharge in supercapacitors | 26 |
| Chapter 3 Experimental | 29 |
| 3.1 X-ray Diffraction..... | 29 |
| 3.2 Brunauer-Emmett-Teller | 31 |
| 3.3 Electrochemical Impedance Spectroscopy | 33 |
| 3.4 Preparation of the cells..... | 37 |
| 3.5 Self-discharge tests..... | 38 |
| 3.6 Float charge current..... | 40 |
| Chapter 4 Results and Discussion..... | 41 |
| 4.1 Studies of self-discharge on the ReHAB..... | 41 |
| 4.2 Effect of different current collectors | 41 |
| 4.3 Effect of Conductive Additive | 44 |
| 4.3.1 Amount of Carbon | 44 |
| 4.3.2 Type of Carbon..... | 45 |
| 4.4 Effect of different state of charge..... | 48 |
| 4.5 <i>Ex-situ</i> X-ray Diffraction Studies of ReHAB | 49 |
| 4.6 Stability of LiMn_2O_4 in the electrolyte | 53 |
| Chapter 5 Conclusions and Future Work..... | 56 |

| | |
|-----------------------|----|
| 5.1 Conclusions | 56 |
| 5.2 Future Work | 57 |
| Bibliography | 59 |

List of Figures

| | |
|--|----|
| Figure 1. 1 Electric vehicle production and lithium demand for electric vehicle batteries, 2008-2020 ¹ | 1 |
| Figure 2. 1 Comparison between volumetric and gravimetric energy density of secondary batteries ²¹ | 5 |
| Figure 2. 2 Li-ion batteries usage and forecast ²⁶ | 6 |
| Figure 2. 3 Working principle schematic of Li-ion batteries | 7 |
| Figure 2. 4 Structures of (a) LiCoO ₂ , (b) LiMn ₂ O ₄ and (c) LiFePO ₄ ⁵² | 12 |
| Figure 2. 5 Accidents with Li-ion batteries | 13 |
| Figure 2. 6 The potentials of the indicated reactions versus the standard hydrogen electrode (SHE) in acidic and basic solutions ⁴ | 14 |
| Figure 2. 7 The potential electrode materials which could be used for aqueous rechargeable lithium-ion batteries ⁵⁶ | 15 |
| Figure 2. 8 Working principle schematic of ReHAB ¹⁵ | 17 |
| Figure 2. 9 (a) Charge-discharge profile of ReHAB, (b) and (c) cycling performance of using non-doped and doped LiMn ₂ O ₄ electrode, respectively ¹⁵ | 18 |
| Figure 2. 10 Schematic of self-discharging cell ⁷⁷ | 19 |
| Figure 2. 11 OCV curves used to determine the electrode composition during aging ⁸² | 21 |
| Figure 2. 12 Schematic illustration of the (a) oxidative electrolyte decomposition at the cathode surface and (b) of a protective SEI layer on the cathode surface ⁸⁴ | 22 |

| | |
|---|----|
| Figure 2. 13 Voltage and Energy drop during the OCV in supercapacitors ⁸⁹ | 27 |
| Figure 2. 14 Schematic diagram of a redox shuttle process ⁸⁹ | 28 |
| Figure 3. 1 (a) geometry for diffraction of x-radiation, (b) relationship of the Bragg angle (θ) and the experimentally measured diffraction angle (2θ) | 29 |
| Figure 3. 2 A schematic of the XRD experiment..... | 30 |
| Figure 3. 3 XRD machine (D8 Discover) | 31 |
| Figure 3. 4 BET machine (ASAP 2020) | 33 |
| Figure 3. 5 Nyquist plot ⁹⁹ | 35 |
| Figure 3. 6 Schematic representations of Li-ion mass transfer phenomena which occur in Li-ion battery electrodes and their respective Nyquist plots ¹⁰⁰ | 36 |
| Figure 3. 7 Schematic of EIS measurement test | 37 |
| Figure 3. 8 (a) Swagelok TM type battery, (b) Schematic of the self-discharge test | 39 |
| Figure 4. 1 Voltage drop over time for three different current collectors..... | 43 |
| Figure 4. 2 Capacity loss versus self-discharge time..... | 43 |
| Figure 4. 3 Stainless steel foil after the test | 44 |
| Figure 4. 4 Voltage drop plateau of (a) 1 day and (b) 3 days of OCV for different amount of carbons..... | 45 |
| Figure 4. 5 Voltage drop plateau of (a) 1 day, (b) 3 days of OCV and (c) float charge current profile, (d) capacity lost over time for different carbons..... | 46 |

| | |
|--|----|
| Figure 4. 6 EIS profile of ReHAB cathodes with different carbons: (a) fresh cell; (b) after charge; (c) after OCV for 1 day; d) after discharge..... | 47 |
| Figure 4. 7 EIS profiles of ReHAB cathode with Super P-Li..... | 48 |
| Figure 4. 8 XRD profile of (a) after discharged, self-discharged and charged cell and (b) PE current collector..... | 50 |
| Figure 4. 9 (a) Voltage drop profile and (b) XRD pattern of self-discharged cell and cell discharged at low rate | 51 |
| Figure 4. 10 Discharge capacity vs cycle number | 52 |
| Figure 4. 11 XRD profile of pure LiMn_2O_4 and soaked LiMn_2O_4 for a week | 54 |
| Figure 4. 12 Float charge current profile at different temperature | 55 |

List of Tables

| | |
|---|----|
| Table 2. 1 Comparisons of cycling properties of ARLB under different test conditions ⁵⁶ | 16 |
| Table 2. 2 Different tested compounds and the corresponding percentage in the base electrolyte solution (1 M LiPF ₆ in EC:DMC, 1:1). The tendency of the influence on the self-discharge is indicated by '+', '0', or '-' for a beneficial, almost none, or a detrimental effect, respectively ⁸⁴ | 22 |
| Table 4. 1 Summary of voltage drop and remained capacity after days of OCV for different amount carbons | 45 |
| Table 4. 2 BET surface areas of different of carbonaceous materials | 46 |
| Table 4. 3 Summary of voltage drop and capacity retention of ReHAB cells after 1 day at OCV at the different SOC..... | 49 |

List of Abbreviations

ReHAB: Rechargeable hybrid aqueous battery

SHE: Standard hydrogen electrode

HF: Hydrofluoric acid

ARLB: Aqueous rechargeable lithium battery

GITT: Galvanostatic Intermittent Titration Technique

OCV: Open circuit voltage

SEI: Solid electrolyte interphase

XRD: X-ray diffraction

BET: Brunauer-Emmet-Teller

EIS: Electrochemical impedance spectroscopy

SS: Stainless steel foil

Gr: Graphite foil

PE: Polyethylene film

KB300: Ketjen Black EC300J

SP-Li: Super P-Li

KS6: KS6 graphite

SOC: State of charge

NMP: 1-methyl-2-pyrrolidinone

PVDF: Polyvinylidene fluoride

SEM: Scanning electron microscopy

Chapter 1 Introduction

In recent years, there has been an increasing demand for high energy density rechargeable batteries for portable electronics and electric and hybrid vehicles applications. Li-ion type batteries are good choices for such applications, as well as for electric power load leveling systems. As it can be seen in Figure 1. 1 the demand for lithium just for electric vehicle batteries will almost triple from 2014 to 2020.

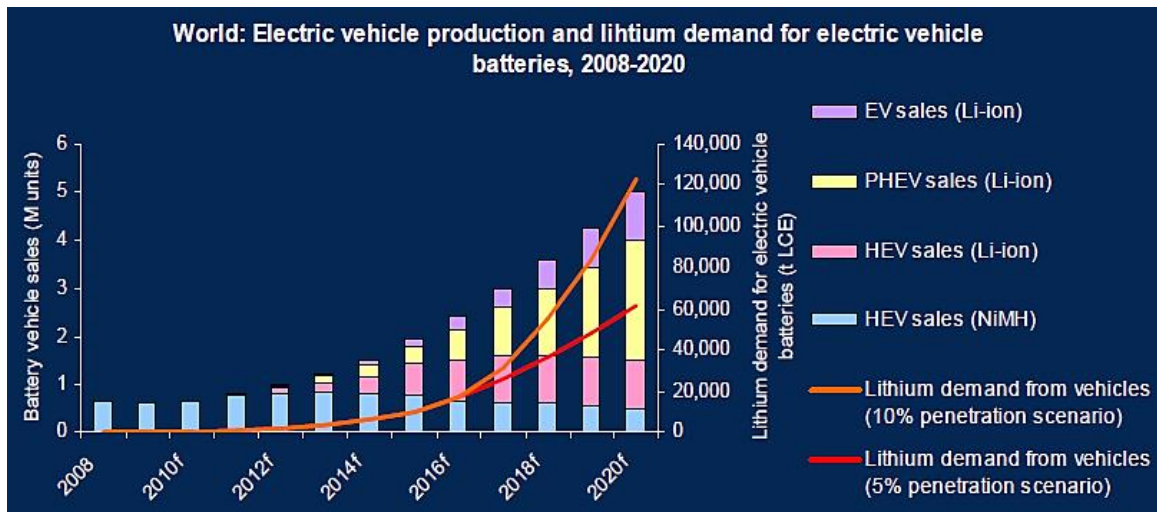


Figure 1. 1 Electric vehicle production and lithium demand for electric vehicle batteries, 2008-2020¹

However, the flammable organic liquid electrolytes used in Li-ion batteries represent a safety hazard.^{2,3} One way to overcome this drawback is to use aqueous electrolytes instead of the flammable organic electrolytes. In addition to improved safety, the ionic conductivity of aqueous electrolytes is typically larger than their organic counterparts. Furthermore, manufacture of Li-ion batteries is complicated and expensive, partly due to the electrolyte being moisture and air sensitive. Thus, incorporation of aqueous electrolytes in rechargeable

lithium batteries greatly reduces production costs by avoiding the strict assembly conditions demanded by the organic electrolytes. An aqueous Li-ion battery based on the same technological concept developed by Sony was first reported by Dahn's group in 1994.⁴ They used VO_2 as a negative electrode and LiMn_2O_4 as a positive electrode in 5M LiNO_3 solution. Despite of its poor cyclability, the prospects of that system instigated many studies of similar aqueous rechargeable lithium-ion batteries. In the following years, various aqueous lithium-ion battery technologies have been developed.⁵⁻¹⁴

A new concept in aqueous rechargeable batteries was developed in Chen's research group.¹⁵ The combined performance attributes of the Rechargeable Hybrid Aqueous Battery (ReHAB) indicates that it constitutes a viable alternative energy storage system, with potential to replace the commercial lead-acid system and can be used for large scale energy storage applications. Commercialization of this technology, however, depends on the investigation of some parameters, one of them being the self-discharge performance of the cell.

In this thesis we have report on the effect of different components of the cathode on the self-discharge performance of the ReHAB battery. This work is aimed to evaluate the causes for self-discharge in the ReHAB battery.

The thesis is divided into 5 chapters:

Chapter 1 provides an overview of the aqueous rechargeable batteries and objective of the research. It also includes the outline of the thesis.

Chapter 2 reviews the literature about traditional Li-ion batteries, their working principles, and cathode materials. Aqueous rechargeable lithium batteries are also appraised. The definition of self-discharge is given and the process in 3 different systems is discussed.

Chapter 3 describes the experimental methodologies and techniques employed in the data collection.

Chapter 4 displays the results obtained and their interpretation.

Chapter 5 presents the main conclusions of the thesis and suggestions for future work.

Chapter 2 Literature Review

2.1 Li-ion Batteries

The existence and sustainable development of our modern society is closely tied to the development of new/renewable energy sources.¹⁶ Nowadays, fossil fuels are the main source of the world's energy. However, the diminishing world reserves and detrimental environmental effects caused by their combustion, has lead researchers to search for a “green” energy source substitute, one that is renewable and carries lower risk to our environment.^{17,18} Wind and solar power meet these requirements, but have the drawback of energy input and output fluctuation. To circumvent the power fluctuation, energy storage devices are often employed in conjunction with intermittent power sources. One of the most common energy storage systems is the lead-acid battery. Lead-acid batteries are cheap, stable in over-charging conditions, and have low internal impedance which allows them to deliver very high currents. On the other hand, lead-acid batteries are very heavy, which prevents their usage in portable electronics, and contain the environmental unfriendly lead. In addition, lead acid batteries have high self-discharge rates at higher temperature. Li-ion batteries have taken much attention of researchers during the last 5 decades. As seen in Figure 2. 1, Li-ion batteries exhibit high volumetric and the highest gravimetric energy density among the technologies available. Li^+/Li has a very negative standard reduction potential of -3.05V versus a standard hydrogen electrode (SHE) which produces higher power and energy density compared with other batteries. As a result, Li-ion batteries meet

many requirements for applications in portable electronic devices, as well as in electric and hybrid/electrical vehicles.^{19,20}

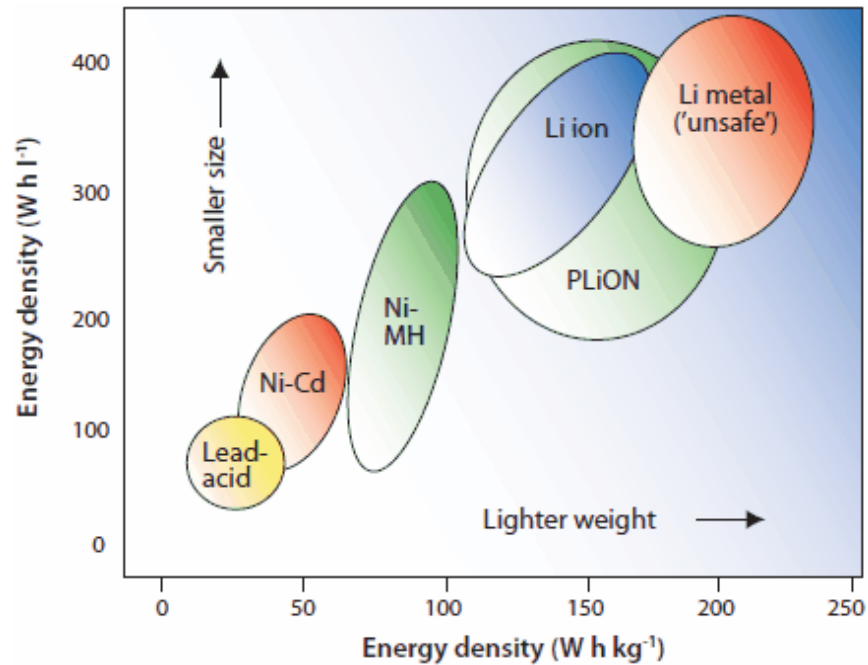


Figure 2. 1 Comparison between volumetric and gravimetric energy density of secondary batteries²¹

In 1991 Sony introduced the commercial lithium-ion battery which is considered the most successful and most widely applied portable energy storage system.^{22,23} The energy density of commercial Li-ion battery is about twice that of nickel–cadmium or nickel– metal hydride batteries, in terms of both weight and volume. In addition, due to the high voltage of Li-ion batteries (about 4 V) it is possible to use a single Li-ion cell to power a cell phone. As shown in Figure 2. 2, the use of the lithium-ion battery has expanded rapidly and it is forecasted to keep increasing over the next 10 years.²⁴ Besides portable electronics, Li-ion

batteries are being increasingly used in electric-powered vehicles, an environmentally friendly mode of transportation expected to grow sharply.²⁵

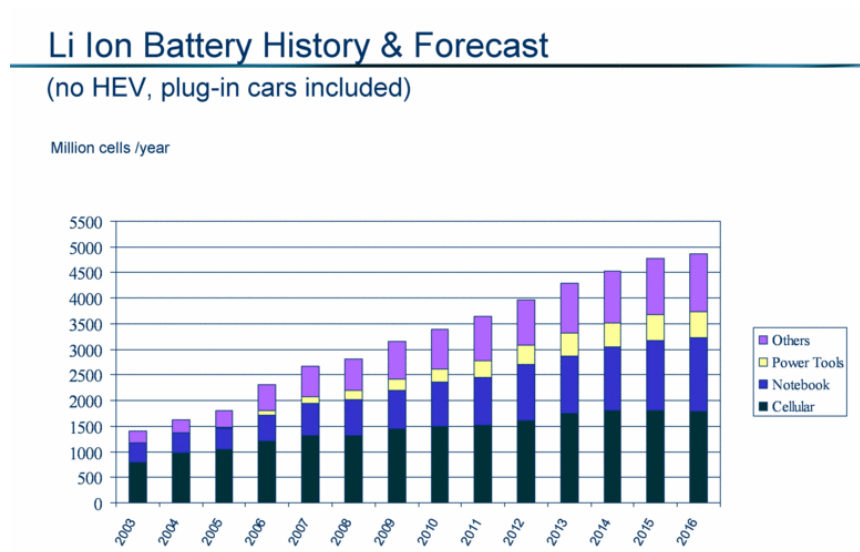


Figure 2. 2 Li-ion batteries usage and forecast²⁶

There are three groups of lithium batteries: lithium metal, lithium-ion and lithium-ion polymer. Lithium metal batteries are not rechargeable whereas lithium-ion and lithium-ion polymer batteries are rechargeable.²⁷ In Li-ion batteries the electrolyte is a lithium salt dissolved in an organic solvent. Li-ion polymer batteries use a solid composite polymer as a separator which contains the lithium salt electrolyte, either soaked in the polymer or as part of its structure.

2.2 Working Principle of Li-ion Batteries

There are three main parts in a battery: an anode (which is oxidized), a cathode (that is reduced) and an electrolyte. When external load is applied to the cell, electrochemical

reduction and oxidation (redox) reactions occur resulting in transfer of electrons from the anode to the cathode. This transfer converts the chemical energy stored in the active material to electrical energy which flows as current through the external circuit. The chemical energy released is determined by the difference between the standard Gibbs free energy chemical potential of the two electrodes. In terms of Li-ion batteries, the redox reactions usually result from the “lithium insertion” or “lithium intercalation” into appropriate hosts. As Figure 2. 3 illustrates, during the charging process Li-ions de-intercalate from the cathode (e.g. LiCoO_2) and intercalate into the anode (e.g. graphite); during the discharge the reverse process takes place.

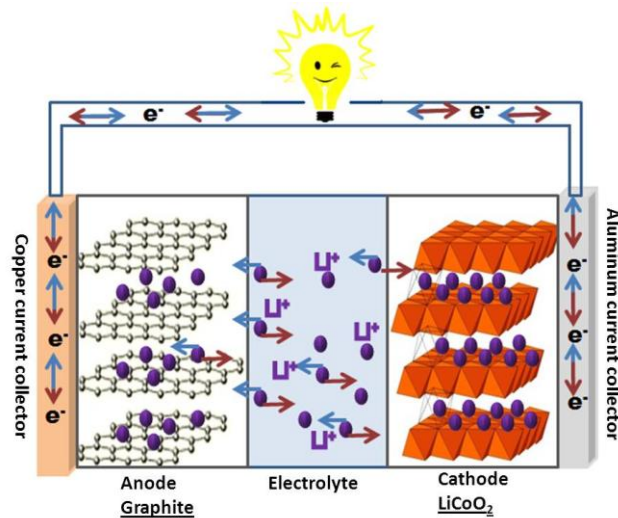
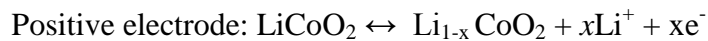
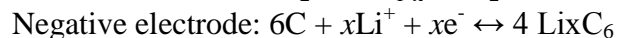


Figure 2. 3 Working principle schematic of Li-ion batteries

The following exemplifies the reactions during the charge-discharge:



Equation 2. 1



Equation 2. 2

The original lithium battery uses metallic lithium as the anode. Despite providing the highest possible energy for the cell, the formations of lithium dendrites during charging can cause short-circuits and represent a safety hazard. In 1991 graphite was introduced as anode to prevent lithium dendrite formation.²⁸ It remains as the anode material of choice even though many alternatives (such as LiTiO, LiVO, etc) have been investigated.²¹

2.2.1 Cathode Materials for Li-ion Battery

The positive electrode in Li-ion batteries is typically a lithium transition-metal chalcogenide that can reversibly de/intercalate Li-ion.^{17,29,30} Presently, three types of cathode electrode materials are predominantly used, namely: layered oxides (lithium cobalt oxide, Figure 2. 4(a)), spinel oxides (lithium manganese oxide, Figure 2. 4(b)) and phosphates (lithium iron phosphate, Figure 2. 4(c)).

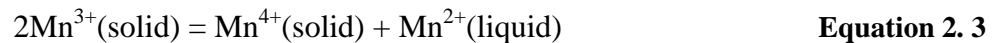
LiCoO₂

Layered LiCoO₂ was developed by Mizushima in 1980, and after successful commercialization, has dominated the lithium batteries market.³¹ Due to the cycling stability, high energy density, and low self-discharge of LiCoO₂ cathode material, it is heavily employed in batteries for laptops, cell phones, and other portable electronics. Li_xCoO₂ has a theoretical capacity of 274 mAh/g if all Li is de-intercalated from the cathode. Unfortunately, this capacity is not practically achievable due to the structure instability of LiCoO₂. As a result, only half of Li can be extracted from the cathode, giving a theoretical capacity of about 140 mAh/g. The high price and toxicity of Co are additional drawbacks of the LiCoO₂

cathode material. To overcome these limitations, Co has been partially substituted in the layered oxide by Mn and/or Ni to form a lithium mixed transition metal oxide (e.g. $\text{Li}(\text{Co}_{0.2}\text{Ni}_{0.8})\text{O}_2$, $\text{LiCo}_{1/3}\text{Ni}_{1/3}\text{Mn}_{1/3}\text{O}_2$, and $\text{LiNi}_{0.5}\text{Mn}_{0.5}\text{O}_2$).^{32,33} Their capacity is about 200 mAh/g and they present better cycling life than the non-substituted layered oxide.^{20,34}

LiMn_2O_4

In 1983 the spinel LiMn_2O_4 was introduced as a cathode material for Li-ion batteries.^{33,35,36} The operating voltage of LiMn_2O_4 is 3.95 – 4.1 V and the theoretical capacity is 148 mAh/g. Because of its high thermal stability, low cost, and low toxicity, LiMn_2O_4 is an excellent candidate to replace LiCoO_2 . However, pure lithium manganese oxide has poor cycling stability and low rate capability. The capacity fading mechanism of the pure lithium manganese oxide has been reportedly related to the Jahn–Teller distortion caused by the presence of Mn^{3+} ions. This phase transition from a cubic into a tetragonal crystal structure is a first order process and occurs first on the surface of some particles but can expand into the full composition of LiMn_2O_4 . Thermodynamically speaking, the system is not at equilibrium. Although small, the distortion is big enough to convert the cubic structure into the lower symmetry and higher disordered tetragonal structure. Additionally, at the end of discharge Mn^{3+} is in high concentration and the following reaction could take place:



When this happens, the Mn^{2+} ions dissolve into the electrolyte and eventually cause loss of active material.³⁷⁻⁴⁰

Two approaches have been proposed to improve the cycling property of LiMn_2O_4 : The first method uses electron doping of LiMn_2O_4 , for example partial substitutions of Mn to make $\text{LiM}_x\text{Mn}_{2-x}\text{O}_4$ (M=Co, Mg, Cr, Ni, Fe, Al, Ti and Zn).⁴¹⁻⁴⁵ Results indicate this approach can effectively stabilize the spinel structure markedly improves the cycling performance of LiMn_2O_4 . However, Mn dissolution is observed as a result of interfacial side reactions between electrodes and electrolytes during the charge/discharge process. This happens when acids like hydrogen fluoride (HF) are formed in the electrolyte due to reactions of electrolyte salt fluorinated anions with trace amounts of waters and/or solvent oxidation products.

The second method constitutes in coating the LiMn_2O_4 with a thin layer of inactive oxide (e.g. ZrO_2 , Al_2O_3 , SiO_2 and MgO).⁴⁶⁻⁵¹ The surface treatment of spinel LiMn_2O_4 decreases the surface area directly in contact with the electrolyte and retards or prevents the side reactions which cause Mn dissolution.

LiFePO₄

In the last 15 years, olivine-type lithium metal phosphates have been intensely investigated as cathodes for rechargeable lithium batteries, in attempts to overcome many of the weaknesses inherent to earlier materials.⁵² Lithium metal phosphates with olivine-structure (phospho-olivines) of general formula LiMPO_4 (M = Fe, Mn, Co, and Ni) were first identified as cathode materials for lithium-ion batteries by Goodenough's team in 1997.⁵³ Olivines require additional treatment with conductive aids to perform at reasonable capacities because of their low conductivity, due to the robust covalent bonding of PO_4^- . However,

phospho-olivines are characterized by nearly flat oxidation-reduction voltage curves, long cycle life, superior resistance to overcharge, higher thermal stability and lower cost than cobalt and manganese oxides. LiFePO_4 is the only commercially available olivine, and must be calcined in an oxygen-free environment where particle surfaces are modified to incorporate a conductive layer of carbon or Fe_3P . LiFePO_4 , in particular, has already found widespread applications in industry due to its reasonable voltage of 3.5 V and theoretical capacity of 170 mAh/g, low cost and low toxicity, and high thermal stability.^{29,30} Because of its substantial potential, much research effort has been directed towards optimizing synthesis routes for LiFePO_4 cathodes. A variety of techniques have been developed to control particle size and morphology and improve the electrical conductivity. However, the practical specific charge capacity of LiFePO_4 is about 130 mAh/g and, because discharge occurs at about 3.5 V vs. Li/Li^+ (lower than for LiCoO_2), it is less attractive for high power applications. On the other hand, this makes the material less reactive towards electrolytes, which reduces specific charge fading. Lithium extraction from LiFePO_4 occurs in the form of a FePO_4 growing shell, and a shrinking LiFePO_4 core. This insertion reaction is a two-phase reaction between FePO_4 and LiFePO_4 . Each of these phases is highly stoichiometric with a very low concentration of mixed-valence states and, therefore, has a poor electric conductivity.^{20,53,54}

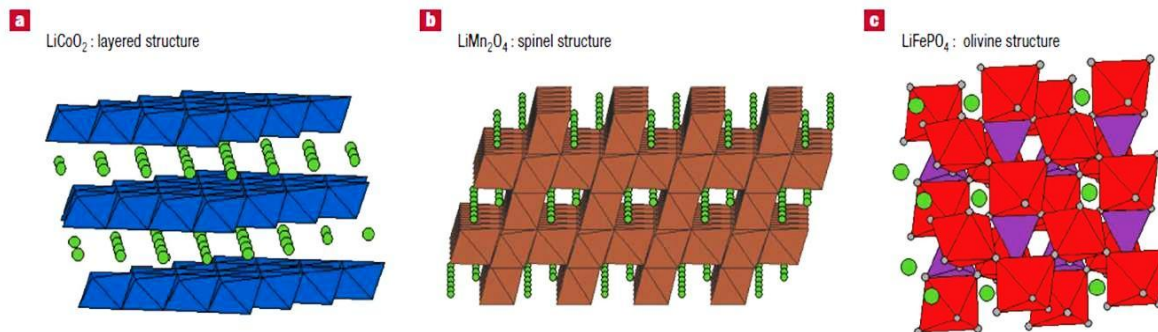


Figure 2. 4 Structures of (a) LiCoO_2 , (b) LiMn_2O_4 and (c) LiFePO_4 ⁵²

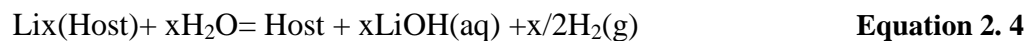
2.3 Aqueous Rechargeable Lithium Batteries

Li-ion technologies lead the battery market, being used in applications from portable electronics to hybrid or electric vehicles. However, some challenges remain in the technology which is especially detrimental for large device applications, one of them being safety. Li-ion batteries use flammable organic electrolytes, which are not stable in air and can easily catch fire. During the 2008 Beijing Summer Olympic incidents caused by explosions of Li-ion cells in battery pack powered electric buses were reported. More recently, in the fall of 2013, a Tesla S car powered by Li-ion batteries caught fire in USA. These incidents (Figure 2. 5) and many others were caused by the liquid electrolyte.² In an attempt to overcome these problems Dahn and co-workers introduced the aqueous lithium rechargeable batteries (ARLB).^{4,13} In addition to better safety, preparation of ARLB cells is cheaper compared to the Li-ion batteries, because there is no need for a controlled environment to handle the aqueous electrolyte.



Figure 2. 5 Accidents with Li-ion batteries

The operational voltage of an ARLB is limited by the potentials for oxygen and hydrogen evolution because of the aqueous electrolyte. Figure 2. 6 show how the potential of oxygen and hydrogen evolution differs by changing the pH of the electrolyte. In the case of Dahn’s cell, LiMn_2O_4 and VO_2 were used as cathode and anode, respectively, and an aqueous 5.0 M solution of LiNO_3 and about 0.001 M in LiOH were electrolytes. Addition of a small amount of base to LiNO_3 solution promoted stabilization of the cathode material by preventing the following side reaction:



The presence of the base also adjusted the standard potential for the system to an average voltage 1.5 V.⁴

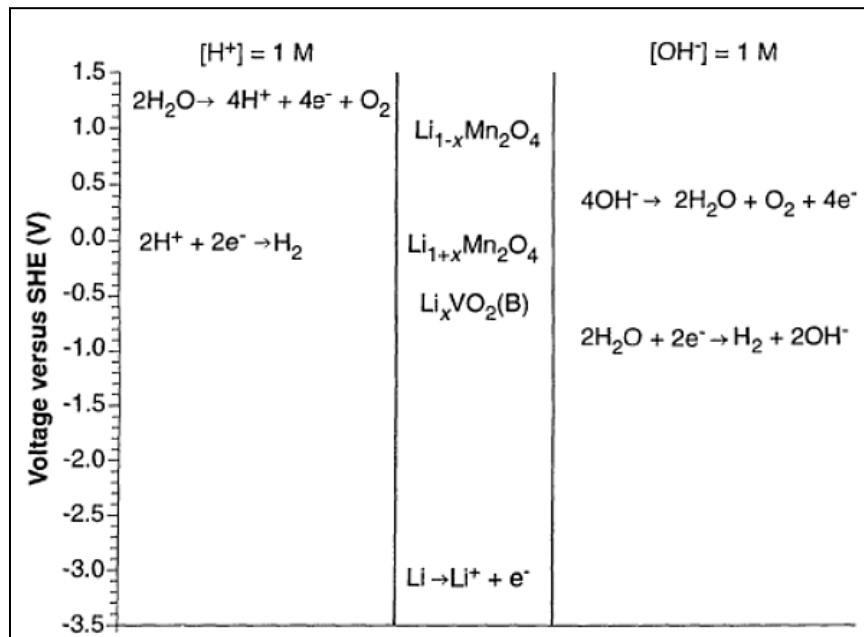


Figure 2. 6 The potentials of the indicated reactions versus the standard hydrogen electrode (SHE) in acidic and basic solutions ⁴

Figure 2. 7 illustrates how the potential for lithium intercalation into cathode materials relates with oxygen and hydrogen evolution.⁵⁵ This diagram aids in the selection of suitable cathode and anodes for ARLB, which could be in the range of 2 to 4 V vs. Li/Li⁺ depending on the pH of the electrolyte.⁴

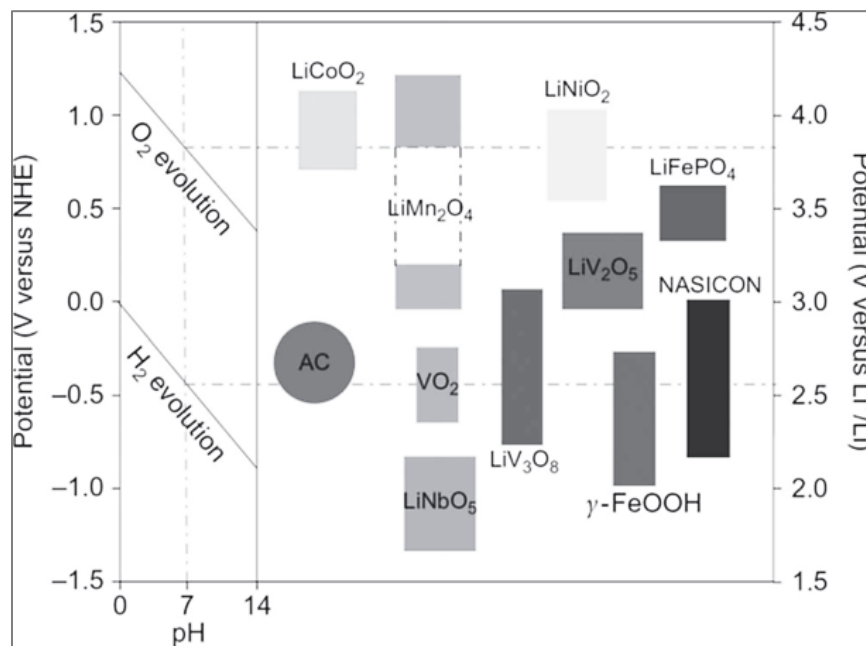


Figure 2. 7 The potential electrode materials which could be used for aqueous rechargeable lithium-ion batteries⁵⁶

After ARLB was introduced, various papers have been published regarding the use of aqueous electrolyte in Li intercalation systems.^{13,57-69} One of them, by Manickan and co-workers, describes the lithium insertion into manganese dioxide electrode in a MnO_2/Zn aqueous battery, using a LiOH solution as an electrolyte.⁷⁰⁻⁷⁶ Their results show that when LiOH is used as an electrolyte, Li intercalated into the cathode upon discharge. This is strikingly different from the traditional alkaline battery, which uses KOH solution as electrolyte and in which the discharge products are MnOOH , Mn_2O_3 or Mn_3O_4 . In a review article, Xia and others have discussed the challenges on ARLB and possible solutions.⁵⁶ One of the problems is the possible reaction of the cathode intercalation compound with oxygen. To mitigate this problem, oxygen should be eliminated from the electrolyte. A comparison of several aqueous battery systems is presented in Table 2. 1. The $\text{LiMn}_2\text{O}_4/\text{AC}$ system shows

excellent cycling performance even at high current density.⁵⁶ However, it has lower energy density than the other systems.

Table 2. 1 Comparisons of cycling properties of ARLB under different test conditions⁵⁶

| Battery system | Current density [mA cm ⁻²] | Charge/discharge rate [C] | Capacity retention [%/# Cycles] |
|---|---|---------------------------------|---------------------------------------|
| LiMn ₂ O ₄ – (B)VO ₂ | 0.69 | 0.1 | Failed/25 |
| LiCoO ₂ – LiV ₃ O ₈ | 3.4 | 1 | 36/100 |
| LiNi _{0.81} Co _{0.19} O ₂ – LiV ₃ O ₈ | 1 | | 40/100 |
| LiMn ₂ O ₄ – TiP ₂ O ₇ | | 0.1 | 37/25 |
| LiMn ₂ O ₄ – LiTi ₂ (PO ₄) ₃ | | 0.1 | 36/25 |
| LiMn ₂ O ₄ – VO ₂ | 60 mAh g ⁻¹ | | 74/50 |
| Li[Ni _{1/3} Co _{1/3} Mn _{1/3}]O ₂ – LiV ₃ O ₈ | 0.2 | | 55/10 |
| LiMn _{0.05} Ni _{0.05} Fe _{0.9} PO ₄ /C – LiTi ₂ (PO ₄) ₃ | 0.2 | | 52/50 |
| LiFePO ₄ – LiTi ₂ (PO ₄) ₃ | 0.1 | 0.125 | 85/50 |
| | 6 | 6 | 90/1000 |
| LiMn ₂ O ₄ /AC | 6 | 10 | 95/20 000 |

2.3.1 Rechargeable Hybrid Aqueous Battery

In an attempt to circumvent the problems associated with the anode side of ARLB, a new system was developed from Chen's research group.¹⁵ The Rechargeable Hybrid Aqueous Battery (ReHAB) consists of a LiMn₂O₄ cathode and Zn foil anode, with a mixture of lithium and zinc chloride aqueous solutions used as electrolyte. It was named hybrid because cycling involves two active species, lithium and zinc ions, which replace each other in the electrolyte. For example when charging the system, Li ions are extracted from the cathode and dissolve into the electrolyte. Concomitantly, Zn²⁺ ions leave the electrolyte and deposit on the Zn foil. The reverse processes occur during the discharge as shown in Figure 2. 8.

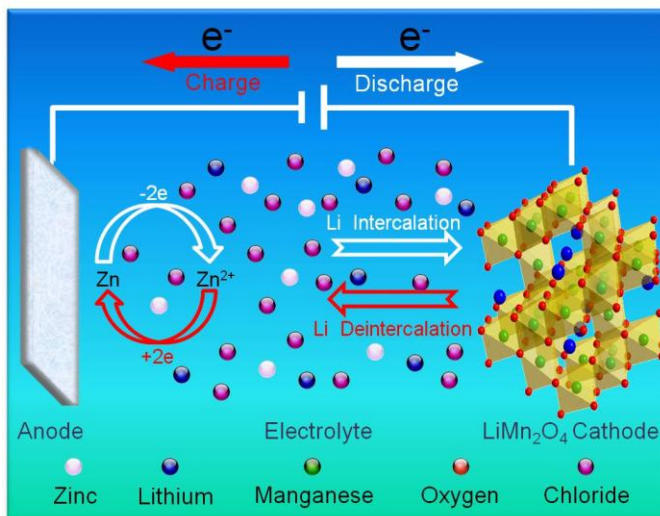


Figure 2. 8 Working principle schematic of ReHAB¹⁵

The charge-discharge profile of the cell (Figure 2. 9(a)) clearly depicts the two-phase de/intercalation reactions of lithium into/from the spinel structure of LiMn_2O_4 . A cell using pure LiMn_2O_4 can be cycled at 4C for 1000 cycles maintaining 95% of the initial capacity (Figure 2. 9(b)). When doped LiMn_2O_4 is used as active material, the cell can sustain 4000 charge/discharge cycles at 4C retaining 95% of the initial capacity (Figure 2. 9(c)). The estimated energy density of the system is 50-80 Wh/kg, which is comparable to traditional aqueous systems such as Lead-acid batteries.

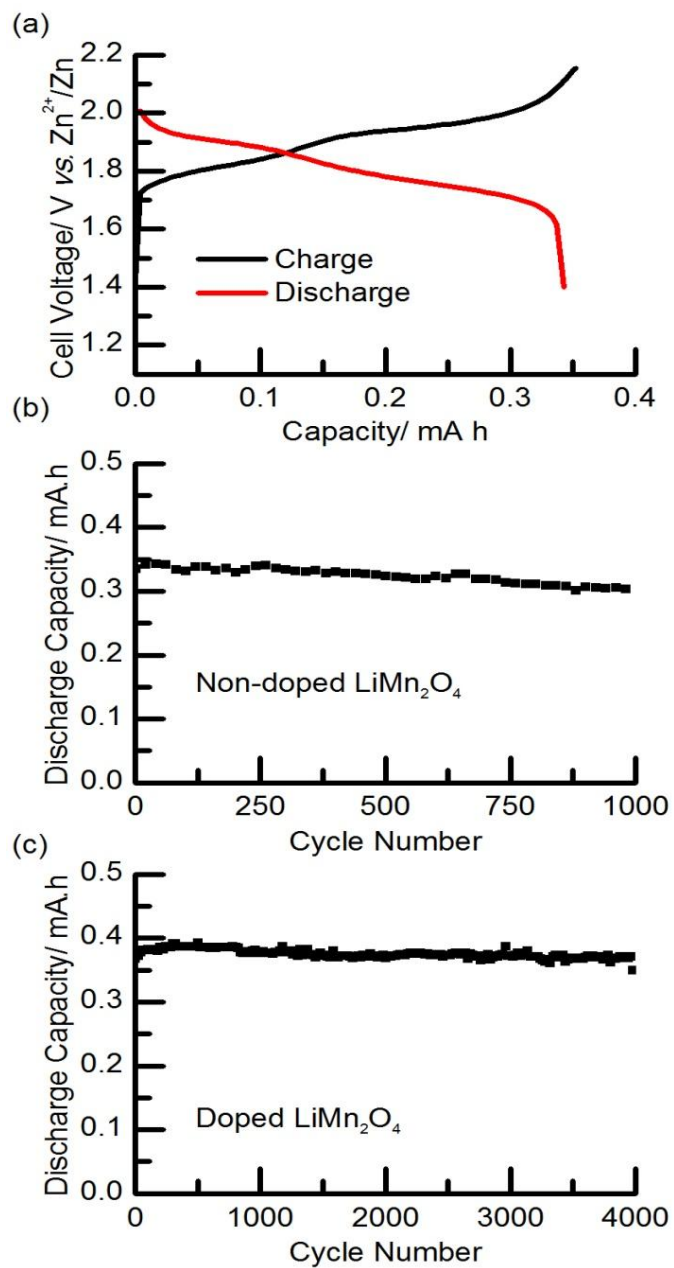


Figure 2. 9 (a) Charge-discharge profile of ReHAB, (b) and (c) cycling performance of using non-doped and doped LiMn₂O₄ electrode, respectively¹⁵

2.4 Self-discharge process

Self-discharge is a process that decreases the capacity of a cell without flow of current through an external circuit. In a simple analogy, as shown in Figure 2. 10, it's like leaking water from a bottle. High self-discharge is a disadvantage for battery systems because they need to be often charged to maintain a full state of charge. Ultimately, high self-discharge of the battery decreases the cell life. For example, if a cell can be cycled to withstand 300 charge/discharge cycles with one daily charge; it can be used for about one year. If the same cell displays high self-discharge, such that it needs to be recharged 2 or 3 times a day, it only lasts for about 4 to 6 months.

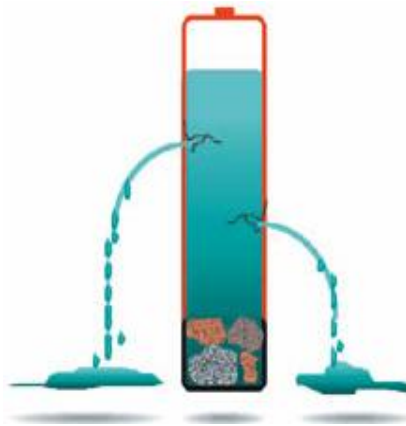


Figure 2. 10 Schematic of self-discharging cell⁷⁷

Self-discharge processes can be tested in a load-free state for a fixed time. For batteries, self-discharge can be evaluated by looking at the capacity loss over time. In the case of supercapacitors, measurement of self-discharge is done by following the voltage decay over time.

2.4.1 Self-discharge in Li-ion Batteries

Charged batteries have high Gibbs free energy, so there is a thermodynamic driving force for self-discharge. Two self-discharge reactions are possible in a Li-ion cell; one is chemical and the other electrochemical. Because of their high reactivity, charged cells can undergo side reactions easily, and factors such as purity of the active material or electrolyte, and the specific surface area of the active electrodes, conductors, binders or separators can have decisive effect on their self-discharge performance. These reactions are mostly irreversible while electrochemical reactions are reversible. For example, lithium re-intercalation can lead to self-discharge of Li-ion batteries, as has been demonstrated by many researchers who have studied all the different factors which could affect self-discharge of these cells.⁷⁸⁻⁸¹

R. Yazami and Y. Ozawa have studied the kinetics of self-discharge in the Li-ion battery using the Galvanostatic Intermittent Titration Technique (GITT) method.⁸² Figure 2. 11 show the GITT at 25°C alongside the open circuit voltage (OCV) data at 70°C. The trends are similar, but during the OCV the potential drops faster at the beginning. The authors concluded that the self-discharge is associated with two factors. The first factor is the lithium re-intercalation into the cathode which is a reversible reaction. The second factor is the phase transition from a spinel to a tetragonal structure, which is an irreversible reaction.

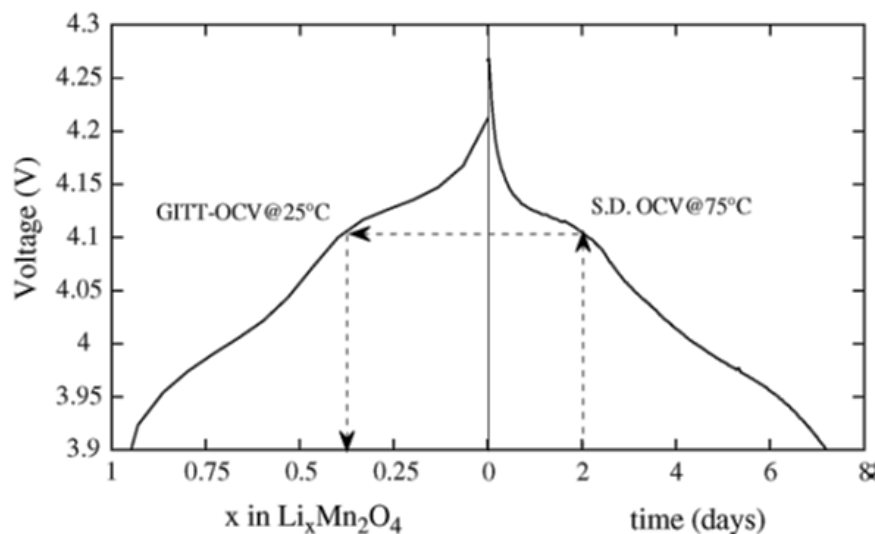


Figure 2. 11 OCV curves used to determine the electrode composition during aging⁸²

In Li-ion batteries self-discharge may occur due to electrolyte decomposition. The decomposition occurs if the electrolyte is not stable at higher potential, since it might oxidize at the cathode or reduce at the anode.^{14,83} Tarnopolskiy et al. studied the influence of 40 different electrolyte additives on the self-discharge of Li-ion batteries (Table 2. 2).⁸⁴ Among the additives, succinic anhydride showed positive influence on the self-discharge. The authors proposed the mechanism shown in Figure 2. 12 to explain the influence of the additive. Figure 2. 12(a) shows that during the open circuit potential, the electrolyte decomposes due to the higher voltage and Li-ions are re-intercalated back to the cathode. The succinic anhydride prevents or thwarts this process by forming a solid electrolyte interphase (SEI) on the surface of the cathode (Figure 2. 12(b)). The SEI will protect the cathode from the re-intercalation and will lower the self-discharge of the cell.

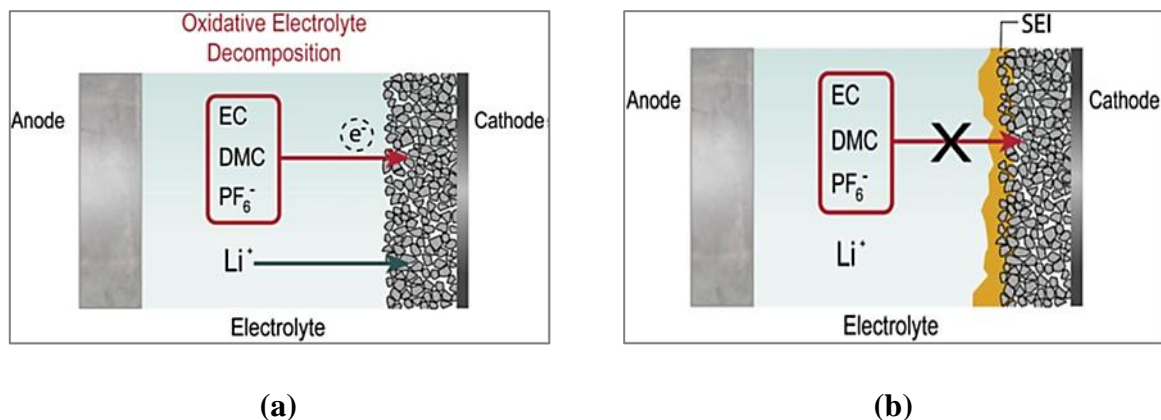


Figure 2. 12 Schematic illustration of the (a) oxidative electrolyte decomposition at the cathode surface and (b) of a protective SEI layer on the cathode surface⁸⁴

Table 2. 2 Different tested compounds and the corresponding percentage in the base electrolyte solution (1 M LiPF₆ in EC:DMC, 1:1). The tendency of the influence on the self-discharge is indicated by '+', '0', or '-' for a beneficial, almost none, or a detrimental effect, respectively⁸⁴

| | Tested compound | Concentration of additive/% | Influence on self-discharge |
|----|--|-----------------------------|-----------------------------|
| 1 | Poly(ethylene glycol) methylether methacrylate | 0.5; 1; 4 | - |
| 2 | Methyl allyl piperidinium-1,3 TFSI | 1; 5; 20 | - |
| 3 | Methylmethacrylate | 1 | - |
| 4 | Pyrrole | 1 | -- |
| 5 | Biphenyl | 0.1 | - |
| 6 | Methyl allylpyrrolidinium FSI | 5 | -- |
| 7 | Methyl allylpyrrolidinium BF4 | 1; 5 | - |
| 8 | Tetrahydrothiophene | 4 | 0 |
| 9 | 3-Bromo-4-methoxy benzonitrile | 1 | - |
| 10 | 4,40-Dimethoxyoctafluorobiphenyl | 1 | - |
| 11 | 5-Chloro-2-methoxypyridinea | 1 | -- |
| 12 | Fluoroethylene carbonate | 4 | 0 |
| 13 | Difluoroethylene carbonate | 4 | 0 |
| 14 | Trifluoroethylene carbonate | 4 | - |

| | | | |
|----|---|----------------------|-----------|
| 15 | Bis(trifluoromethyl)ethylene carbonate | 4 | 0 |
| 16 | 1,3-Propane sultone | 4 | 0 |
| 17 | Tris(trimethylsilyl)borate | 2; 5 | 0 |
| 18 | Tris(trimethylsilyl)phosphite | 2; 5 | 0 |
| 19 | Trimethylsilyltriflate | 4 | – |
| 20 | Bis(trimethylsilyl)malonate | 4 | – |
| 21 | Ethylmethylsulfone | 4 | 0 |
| 22 | Dimethyl sulfone | 4 | 0 |
| 23 | Methyl methanesulfonate | 4 | 0 |
| 24 | Sulfolane | 4 | 0 |
| 25 | 1,3,2-Dioxathiolane 2,2-dioxide | 4 | -- |
| 26 | Tetramethoxytitanium | 4 | – |
| 27 | 1,2-Propyleneglycol sulfite | 4 | – |
| 28 | Lithium bis(oxalate)borate (LiBOB) | 4 | – |
| 29 | Lithium difluoro(oxalate)borate | 4 | – |
| 30 | Tetrafluorosuccinic anhydride | 4 | – |
| 31 | Ethylene sulfite | 4 | – |
| 32 | Succinic anhydride | 1; 2; 4; 6; 8 | ++ |
| 33 | Methyl succinic anhydride | 0.5; 4; 8 | 0 to + |
| 34 | Diglycolic anhydride | 6 | – |
| 35 | Maleic anhydride | 1; 4 | – |
| 36 | 2,2-Dimethyl succinic anhydride | 1 | |
| 37 | 2-(Trifluoroacetamido) succinic anhydride | 0.5 | – |
| 38 | 2-Methylene succinic anhydride | 0.5 | – |
| 39 | Nonenylsuccinic anhydride | 0.5 | -- |
| 40 | Dodecenylsuccinic anhydride | 0.5 | -- |

Effect of Carbons on self-discharge in Li-ion batteries

Carbons play an important role on self-discharge of the cell, due to surface area and particle size. Takashi Utsunomiya and co-workers have studied different carbons as a negative electrode, in order to see how they influence on self-discharge of the battery.⁸⁵ Three carbons were chosen: hard carbon (HC), artificial flake graphite (AFG) and spherical natural graphite (SNG) with surface area of 3.1 m²/g, 21.7m²/g and 3.4m²/g, respectively. Batteries were assembled using these carbons as a negative electrode, and then self-discharge of the cells was identified from the open circuit voltage, capacity loss of the cell during the storage period. From the charge/discharging profiles, they have observed that the columbic efficiency of first cycle for hard carbon was lower than those of two other carbons. This indicates the irreversible capacity of hard carbon would be based not only on the SEI formation but also on the loss of lithium species inside the carbon material. From these results they have concluded that the self-discharging rate was in the order of AFG < HC < SNG for every storage temperature. This order of the self-discharging rate at the same temperature relates to the specific surface area of the carbons. Therefore higher specific surface area and higher storage temperature lead to higher self-discharging rate. They also have studied graphite with different particle sizes.⁷⁹ From the results at high temperature the graphite with smaller particle size showed higher self-discharge rate.

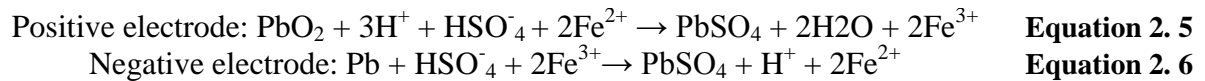
2.4.2 Self-discharge in Lead-acid batteries

Lead–acid batteries are related to the ReHAB systems in many aspects, namely:

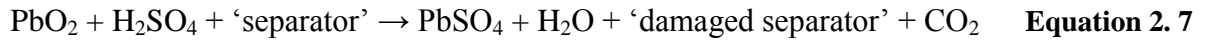
1. As in the ReHAB, the electrolyte is an acidic sulfate based aqueous solution;
2. Lead-acid batteries use the same separator;
3. The anode operates under a dissolution/deposition process;
4. Oxygen and hydrogen evolution are significant side reaction processes.

The first reports about self-discharge of lead-acid batteries were published in 1882.⁸⁶ The positive and negative electrodes of lead-acid batteries are not very stable in the acidic electrolyte. The discharged electrodes (lead sulfate) are more stable than the charged state⁸⁶. In lead-acid batteries, a process called “sulfation” which causes self-discharge has been identified.⁸⁷ During cell discharging, lead sulfate is produced and if the cell is deeply discharged it would be very difficult to convert lead sulfate back to the lead or lead oxide. During storage, lead reacts with electrolytes and forms lead sulfate, which is hard to remove from the surface of negative electrodes.^{87,88} To prevent this reaction, additives (such as boric acid, citric acid and stearic acid) must be added to the electrolyte. Alternatively, stable lead alloys are employed in place of pure lead as anode materials. Small amounts of Sb, Ca, Sn, Al and Ag metals are alloyed with lead, to make for better negative electrodes.⁸⁹

Wenzl has described another side reaction in lead-acid batteries.⁹⁰ It is called the redox-shuttle reaction and occurs when impurities (such as iron) are present in the electrolyte or electrode. The following reactions may take place during the open circuit potential:



Additionally, PbO_2 can also react with the separator producing carbon dioxide, as described by the following reaction:



Hence, although not as strict as lithium ion batteries, the manufacture of lead-acid cells demands careful attention to details; since there are many factors that can affect the self-discharge characteristics.

2.4.3 Self-discharge in supercapacitors

Electrochemical capacitors (ECs), also called supercapacitors or ultracapacitors, are charge storage devices similar to batteries. Charge can be store in a Faradaic reaction as pseudo-capacitance or on the interphase of an electrode/electrolyte as double layers. In double layer EC, carbons with high surface area are used as electrode materials. The high surface area is very important because charge storage depends on it. However, double layer EC have lower energy density compared with pseudo-capacitive EC and batteries.

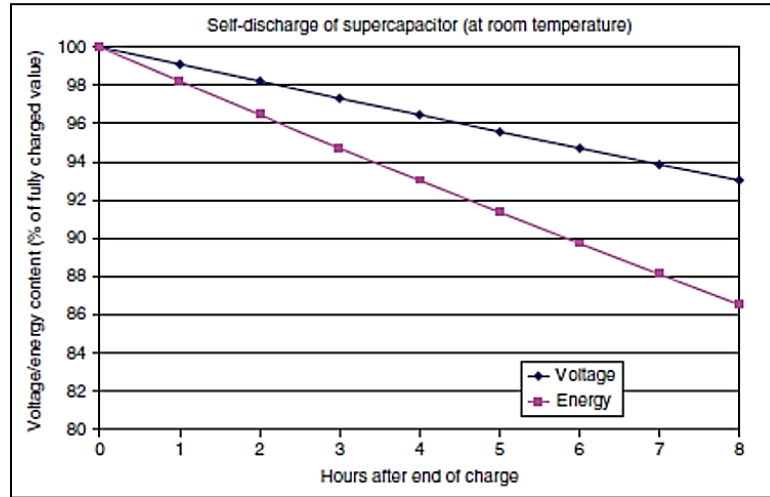


Figure 2. 13 Voltage and Energy drop during the OCV in supercapacitors⁹⁰

The self-discharge process in ECs is similar to that of batteries. Self-discharge is the spontaneous decline in voltage over time (Figure 2. 13).⁹⁰⁻⁹² Conway et al. proposed three mechanisms through which self-discharge of energy storage devices may occur, he also derived models which describe the predicted voltage profile for each mechanism:^{90,93}

(i) An activation-controlled Faradaic process, where the decline of voltage (V or V_t) versus log time would give a straight line:

$$V = -\frac{RT}{\alpha F} \ln \frac{\alpha F i_0}{RT C} - \frac{RT}{\alpha F} \ln t + \frac{C\tau}{i_0} \quad \text{Equation 2. 8}$$

$$V_t = V_i - A \log(t + \tau) \quad \text{Equation 2. 9}$$

A, F, R – constants; **C** – capacitance; **i_0** – exchange current density

T – absolute temperature, **α** – charge transfer coefficient,

t – time, **τ** – an integration constant, **V_i** – initial charging potential

This model describes the self- discharge due to the Faradaic reaction of a species which is either at high concentration in the cell (e.g. electrolyte decomposition) or is attached to the surface (e.g. oxidation/reduction of a carbon surface functionality).

(ii) A diffusion controlled Faradaic process where the potential would decline with the square root of t :

$$V_t = V_i - \frac{2zFAD^{1/2}\pi^{1/2}c_0}{C} t^{1/2} \quad \text{Equation 2. 10}$$

D – the diffusion coefficient of the redox species,

z – the charge, c_0 – the initial concentration, A – the electro active area.

Small amounts of impurities in electrolytes would cause the redox shuttle reaction, by moving from one electrode to the other. (e.g. an Fe shuttle reaction) (Figure 2. 14).

(iii) Ohmic leakage currents or a ‘short circuit’ cause the discharge of the cell even when there is no external current flowing. This type of leakage occurs because of impurities or some mistakes made while producing the cells.

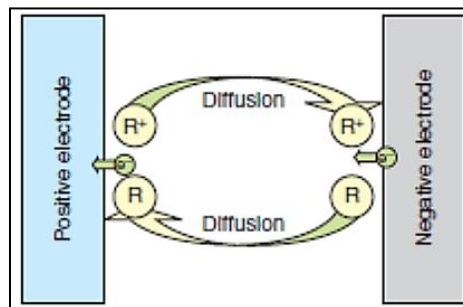


Figure 2. 14 Schematic diagram of a redox shuttle process ⁹⁰

Chapter 3 Experimental

3.1 X-ray Diffraction

X-ray diffraction (XRD) is a widely used technique to determine the crystal structure of materials. Diffraction occurs when radiation is scattered by a regular array of scattering centers. The mechanism of scattering can be explained as the interaction of a photon of electromagnetic radiation with an electron in an atom. Because the wavelength of x-rays is in the same range as chemical bonds, the atoms in a crystalline structure act as the scattering center. Figure 3. 1(a) shows the conditions for diffraction x-rays by a simple crystal lattice, which are governed by Bragg's law:

$$n\lambda = 2d\sin\theta \quad \text{Equation 3. 1}$$

d – the spacing between two adjacent planes of atoms, n – the order of diffraction,

λ – the wavelength of the electromagnetic radiation, θ – the scattering angle.

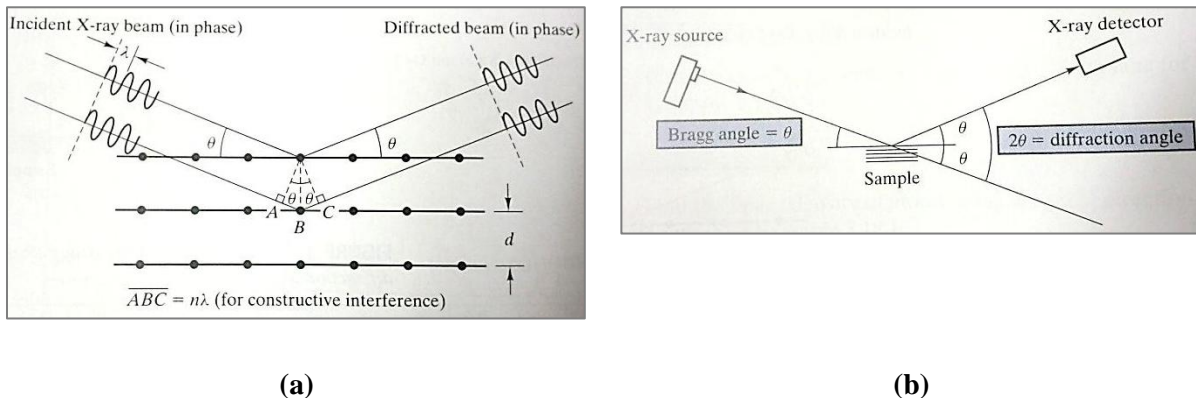


Figure 3. 1 (a) geometry for diffraction of x-radiation, (b) relationship of the Bragg angle (θ) and the experimentally measured diffraction angle (2θ)

The angle θ is also called the Bragg's angle and 2θ is referred to as the diffraction angle (which is experimentally measured) (Figure 3. 1(b)). The magnitude of the interplanar spacing is related to the Miller indices for the plane (h, k, l), which are the reciprocal of the cartesian coordinates of the plane. For instance, the relationship of the cubic system is:

$$d_{hkl} = \frac{a}{h^2 + k^2 + l^2} \quad \text{Equation 3. 2}$$

a – the lattice parameter

The schematic of the experiment in XRD is shown in Figure 3. 2. The diffraction patterns of the samples are recorded through the scanning radiation detector to the computer. Afterwards, the sample profiles can be analyzed by the computer software comparing it to a large collection of known diffraction patterns.⁹⁴

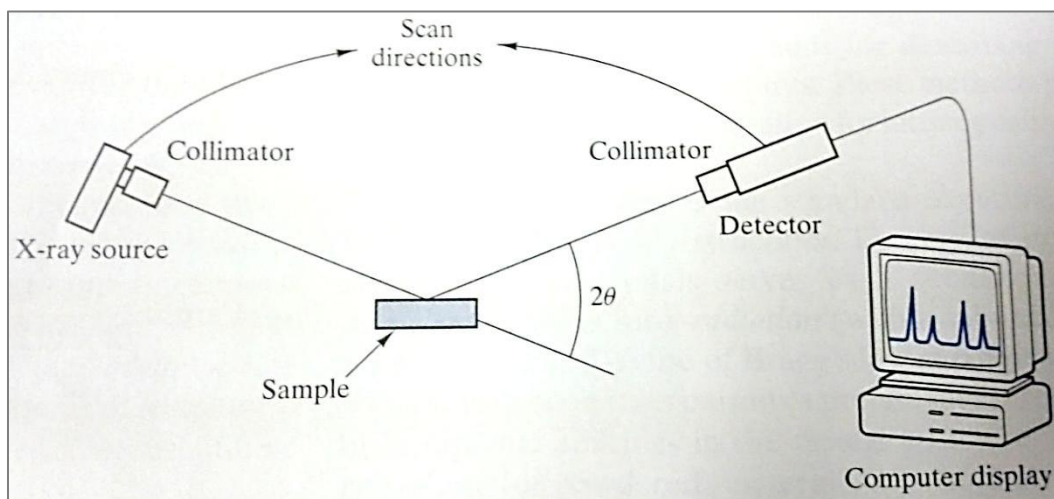


Figure 3. 2 A schematic of the XRD experiment

In this work, XRD (D8 Discover, Bruker Co)(Figure 3. 3) using Cu Ka 1.5418 nm and LynxEye detector was used to determine the LiMn_2O_4 crystalline structure. Charged,

discharged or self-discharged batteries were disassembled and cathode electrodes were removed. Washed with deionized water, dried cathode electrodes were then scanned from 10° to 80° degree with 0.05° degree increments.



Figure 3. 3 XRD machine (D8 Discover)

3.2 Brunauer-Emmett-Teller

Brunauer-Emmett-Teller (BET) is the most common method used to analyze the surface area, porosity and pore distribution of micro and mesoporous materials.^{95,96} The technique is based on the physical adsorption of nitrogen or helium at low, constant temperatures. By measuring the gas uptake (adsorption) upon increasing partial pressure of the gas over a dry powder sample, and the release of gas (desorption) at decreasing partial

pressures, the surface area of the sample can be determined. The main equations governing this method are the following:

$$\frac{1}{W \left(\frac{P_0}{P} - 1 \right)} = \frac{1}{W_m C} + \frac{C - 1}{W_m C} \frac{P}{P_0} \quad \text{Equation 3. 3}$$

W – molecular weight of gas adsorbed

P/P₀ – relative pressure

W_m – weight of adsorbate as monolayer

C –BET constant

From the plot $1/[W(P/P_0)-1]$ against P/P_0 , one can calculate W_m , which is equal to

$$W_m = \frac{1}{(s + i)} \quad \text{Equation 3. 4}$$

where “**s**” is the slope and “**i**” is the intercept of the curve. The the total surface area can then be calculated from:⁹⁷⁻⁹⁹

$$S_t = \frac{W_m N A_{cs}}{M} \quad \text{Equation 3. 5}$$

N - Avogadro's number (6.023×10^{23})

M - Molecular weight of adsorbate

A_{cs} - Adsorbate cross sectional area (16.2 \AA^2 for Nitrogen)

The specific surface area of the sample is a ratio of the total surface area and the weight of the sample:

$$S = \frac{S_t}{w} \quad \text{Equation 3. 6}$$

In this thesis, BET (Figure 3. 4) was used to determine the specific surface area of the different carbonaceous materials, which were used as conductive agents. Liquid nitrogen (boiling temperature of 73K) was used as the adsorbate. Before measurement, all of the samples were degassed at 303K for one hour.



Figure 3. 4 BET machine (ASAP 2020)

3.3 Electrochemical Impedance Spectroscopy

Electrochemical Impedance Spectroscopy (EIS), also known as AC impedance methods, are widely used to characterize the electrode processes and complex interfaces. EIS is an experimental technique which measures the small sinusoidal (AC) current (or voltage) signal of known amplitude and frequency (the perturbation) to an electrochemical cell at a

steady bias potential (or current). EIS is also used to monitor AC amplitude and phase response of the cell. From the measurement information about the interface, its structure and reactions taking place can be inferred. Equivalent circuit analysis of the EIS response provides information on electrode properties like bulk resistance, charge transfer resistance, diffusion and double layer capacitance, etc.^{100,101} The following equation shows the relationship between AC voltage and frequency:

$$E_t = E_0 \sin(\omega t) \quad \text{Equation 3. 7}$$

E_t – the potential at the time t , E_0 – the amplitude of the signal, ω – the angular frequency. Angular frequency ω (expressed in radians/second) can be associated with the frequency f (expressed in hertz):

$$\omega = 2\pi f \quad \text{Equation 3. 8}$$

In a linear system, the response signal can be described as:

$$I_t = I_0 \sin(\omega t + \varphi) \quad \text{Equation 3. 9}$$

Combining equations 3.7, 3.8 and 3.9 into Ohm's Law, the impedance of the system can be calculated as:

$$Z = \frac{E_t}{I_t} = \frac{E_0 \sin(\omega t)}{I_0 \sin(\omega t + \varphi)} = Z_0 \frac{\sin(\omega t)}{\sin(\omega t + \varphi)} \quad \text{Equation 3. 10}$$

Using Euler's relationship:

$$\exp j\alpha = \cos\alpha + jsin\alpha \quad \text{Equation 3. 11}$$

the impedance can be treated as a complex function:

$$Z \omega = \frac{E}{I} = Z_0 \exp -j\varphi = Z_0(\cos\varphi - jsin\varphi) \quad \text{Equation 3. 12}$$

Hence, the EIS measurements can be represented graphically through relations between the imaginary and real parts of the impedance (Figure 3. 5). This plot is known as the “Nyquist or Argand plot”, where the low frequency data is shown on the right and high frequency data is shown on the left. The angle between the vector Z and the x-axis is known as the phase angle.

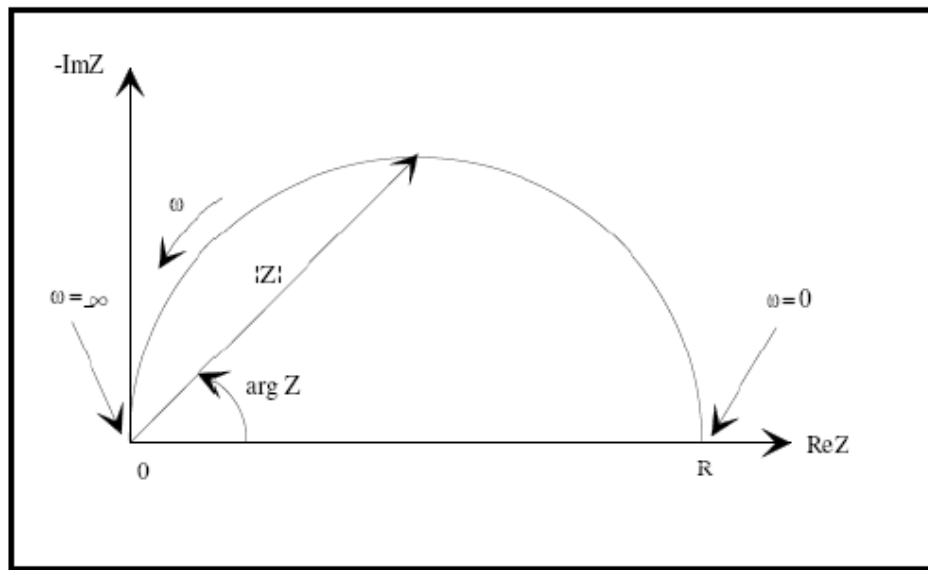


Figure 3. 5 Nyquist plot¹⁰⁰

Figure 3. 6 shows the correlation between the frequencies (time domain) with the physical phenomena taking place in Li-ion batteries.¹⁰¹

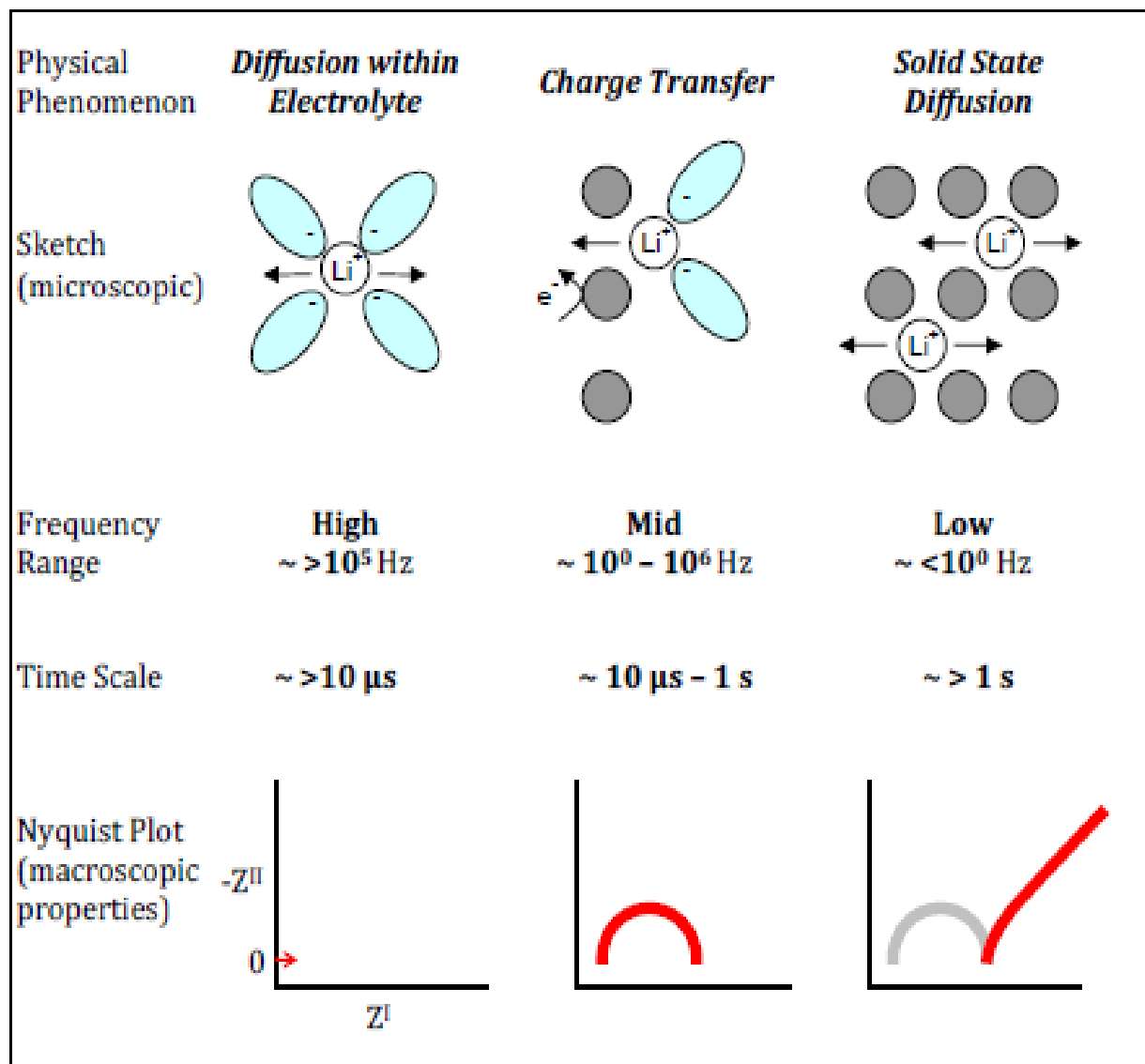


Figure 3. 6 Schematic representations of Li-ion mass transfer phenomena which occur in Li-ion battery electrodes and their respective Nyquist plots¹⁰¹

EIS measurements were performed over the frequency range from 0.1 Hz to 1.0 MHz (VMP3 potentiostat/galvanostat, Bio-Logic Instruments) using the Swagelok™ type cells, as shown in Figure 3. 7.

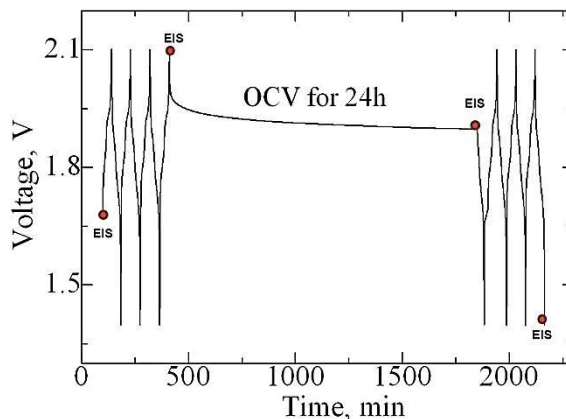


Figure 3. 7 Schematic of EIS measurement test

3.4 Preparation of the cells

Composite cathodes were prepared by mixing 80 wt% of LiMn_2O_4 (MTI Corporation), 10 wt% conductive additives (Super P-Li and KS6 Graphite from Timcal, and Ketjen Black, EC300J, Akzo Nobel) and 10 wt% polyvinylidene fluoride (PVDF, Kynar, HSV900) binder. All components were dispersed in N-methyl-2-pyrrolidone (NMP, Sigma-Aldrich, 99.5% purity) and mixed by Planetary Centrifugal Mixer “Thinky Mixer” (AR-100, THINKYUSA) for 2 minutes. The resulting slurry was cast on a current collector, namely graphite foil (Alfa Aesar, 99.8% (metal basis)), stainless steel (Thin Metal Sales), or conductive polyethylene film (All-Spec), and then vacuum dried at 60°C for a maximum of 12 hours. Cathode discs of 12 mm diameter were then cut out of the film and soaked in the

electrolyte solution under reduced pressure to ensure complete wetting of the material. Swagelok™ type (Figure 3. 8a) cells were assembled, using wet cathode disc, zinc metal discs as anode, and absorbed glass mat (AGM, NSG Corporation) separator wetted with the electrolyte. The mixture of 2M ZnSO₄ and 1 M Li₂SO₄ solutions with pH=4 were used as the liquid electrolyte.

3.5 Self-discharge tests

Self-discharge performance tests of the ReHAB cells were performed at room temperature in Swagelok™ type cells using a computer controlled battery tester (BTS5V5mA, Neware). The cells were galvanostatically cycled for three cycles using 0.25 C equivalent rate ($1C = 130 \text{ mAh g}^{-1}$) between 1.4 and 2.1 V vs. Zn/Zn⁺² for three cycles, charged to 2.1V, then at a charge state left in open circuit voltage (OCV) for 1 day with continued monitoring of the cell voltage. After the OCV period, the cells were discharged to 1.4V and then cycled for another three cycles, to determine the amount of capacity lost during the self-discharge and whether or not this loss is reversible. The schematic representation of the self-discharge test is shown in Figure 3. 8(b).

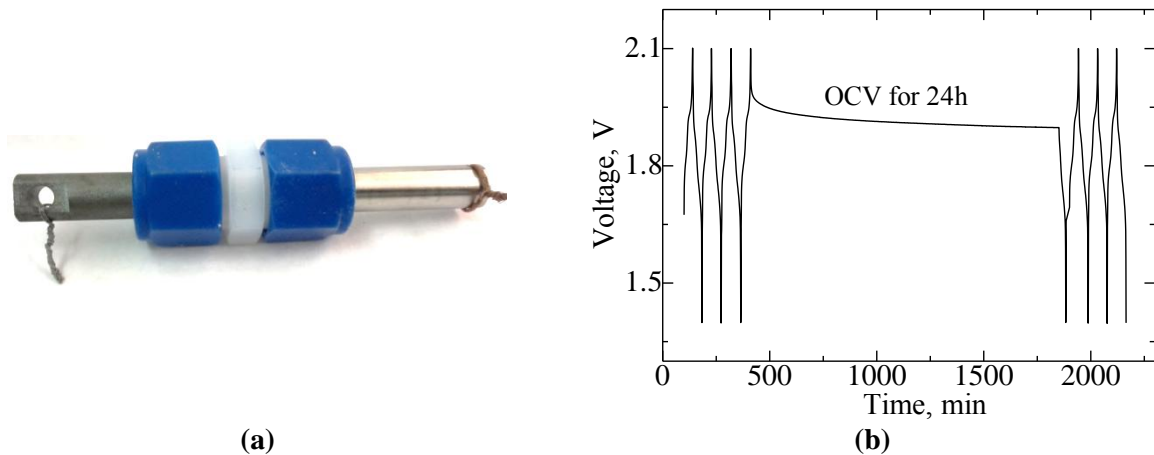


Figure 3. 8 (a) Swagelok™ type battery, (b) Schematic of the self-discharge test

For all experiments, the batteries were assembled as described above, the differences in the cathode composition and the cell structures are summarized in the following tables:

Effect of different state of charge

| Active material | Conductive agent | Binder | Act.mat : Cond.ag.: Bind. | Current collector |
|----------------------------------|------------------|--------|---------------------------|-------------------|
| LiMn ₂ O ₄ | Super P-Li | PVDF | 90:5:5 | Polyethylene film |

Effect of current collector

| Active material | Conductive agent | Binder | Act.mat : Cond.ag.: Bind. | Current collector |
|----------------------------------|------------------|--------|---------------------------|----------------------|
| LiMn ₂ O ₄ | Super P-Li | PVDF | 80:10:10 | Stainless steel foil |
| | | | | Graphite foil |
| | | | | Polyethylene film |

Effect of different amount of active material

| Active material | Conductive agent | Binder | Act.mat : Cond.ag.: Bind. | Current collector |
|----------------------------------|------------------|--------|---------------------------|-------------------|
| LiMn ₂ O ₄ | Super P-Li | PVDF | 80:10:10 | Polyethylene film |
| | | | 85:7.5:7.5 | |
| | | | 90:5:5 | |

Effect of different conductive agents

| Active material | Conductive agent | Binder | Act.mat : Cond.ag.: Bind. | Current collector |
|----------------------------------|-------------------------|---------------|--------------------------------------|--------------------------|
| LiMn ₂ O ₄ | KS6 Graphite | PVDF | 90:5:5 | Polyethylene film |
| | Super P-Li | | | |
| | Ketjen Black 300 | | | |

3.6 Float charge current

A float charge current test was performed by charging the cell to 2.1V and holding it at that voltage for 24 hours, after which the current drop was recorded.

Chapter 4 Results and Discussion

4.1 Studies of self-discharge on the ReHAB

No data is yet available on the self-discharge properties of ARLB. Given the novel character of the ReHAB technology and consequent lack of information on the possible mechanisms involved in the self-discharge, there was the need to look into the self-discharge behavior of different systems like Li ion batteries, lead-acid batteries and supercapacitors, in order to compare the results found from the ReHAB system. In the studies presented herein, the effect of different parts of the cathode (including current collectors) on the ReHAB self-discharge properties were investigated.

4.2 Effect of different current collectors

An electrode current collector can play a significant role in the various self-discharge processes, especially in flood batteries (cells with the electrodes immersed in liquid electrolytes).¹⁰² Since the current collector may get in contact with the electrolyte solution, risk of side-reactions is augmented. In this study, three different current collectors were investigated: stainless steel foil (SS), graphite foil (Gr) and polyethylene film (PE).

Figure 4. 1 illustrates the self-discharge performance of cells with different current collectors that were kept in the OCV condition for several days. As depicted in Figure 4. 2, the cells with SS exhibit significantly more capacity loss (46 % and 66 % after 3 and 15 days respectively) than the cells with graphite and PE. Visual observation of the electrodes, as

seen in Figure 4. 3 revealed that the edges of SS are tarnished, indicative of a corrosion process taking place. The acidic character of the electrolyte used and presence of iron in the stainless steel account for the corrosion side reactions, which are likely responsible for the poor self-discharge performance of the cells with SS current collectors.

The cells using the graphite current collector exhibited improved performance than those with SS, but also deteriorated more than those using polyethylene. The graphite foil grade was 99.7% metal basis, with 100 ppm of leachable chlorides which are likely iron type contaminant. It is inferred that these contaminants may be responsible for the side reactions with electrolytes, which caused some long term capacity loss.

Despite the contribution from the current collectors observed by the different behavior of the cells, the initial overall trend is similar for all three collectors, with a common large voltage drop observed almost immediately at the beginning of the OCV periods. Hence, other mechanisms must play a role on the ReHAB self-discharge. Based on the results presented thus far, the PE current collector was selected in order to begin the evaluation of other factors.

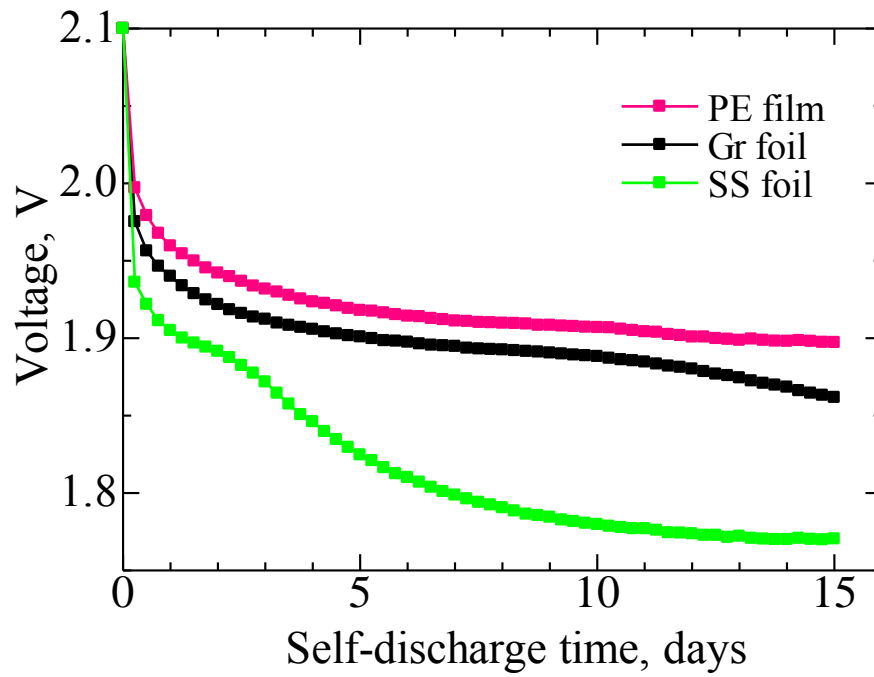


Figure 4. 1 Voltage drop over time for three different current collectors

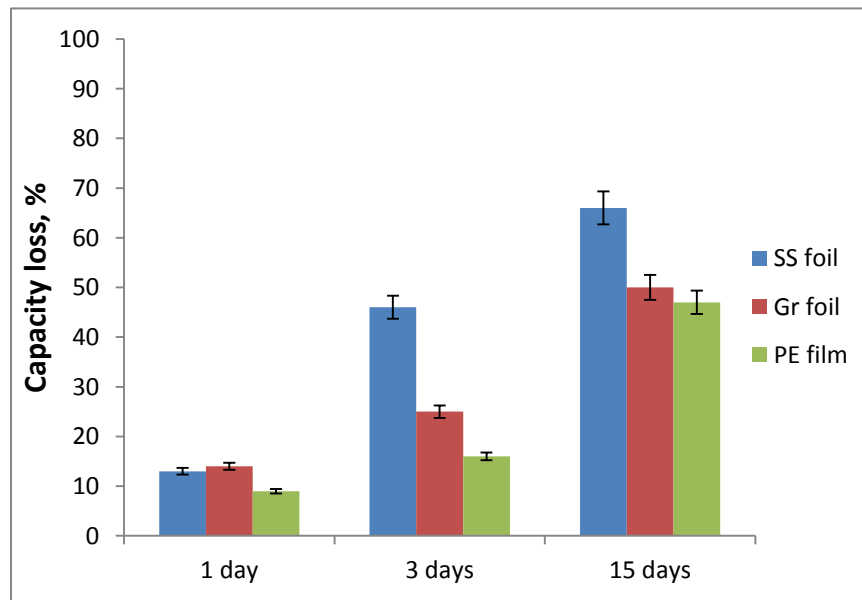


Figure 4. 2 Capacity loss versus self-discharge time

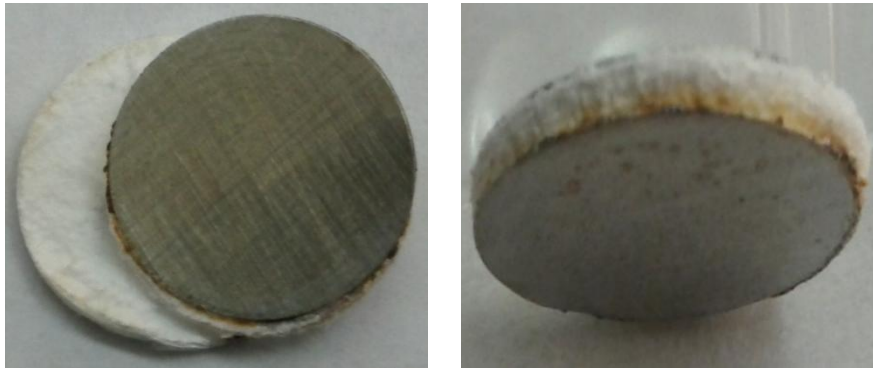


Figure 4. 3 Stainless steel foil after the test

4.3 Effect of Conductive Additive

4.3.1 Amount of Carbon

The effects of the amount of conductive additive in the cathode on the ReHAB self-discharge properties were studied. In these tests, Super P-Li and the ratio of conductive additive to the binder was kept constant at 1:1. Figure 4. 4 show the typical voltage drop over time of ReHAB cells with different amounts of active material, during OCV conditions. The cells containing 5% of carbon performed better than those with 7.5% and 10%, and the difference increases gradually over time. Carbonaceous materials have quite large surface areas which make them more prone to undergo side reactions.⁸¹ Evaluation of the self-discharge rate of ReHAB cells using carbon of different surface area is thus needed and is presented in the following session. Based on the data presented so far, it can be concluded that by reducing the amount of conductors, the self-discharge of the cells could be reduced (Table 4. 1). The lowest level of 5% carbon was then adopted for the remainder of the tests.

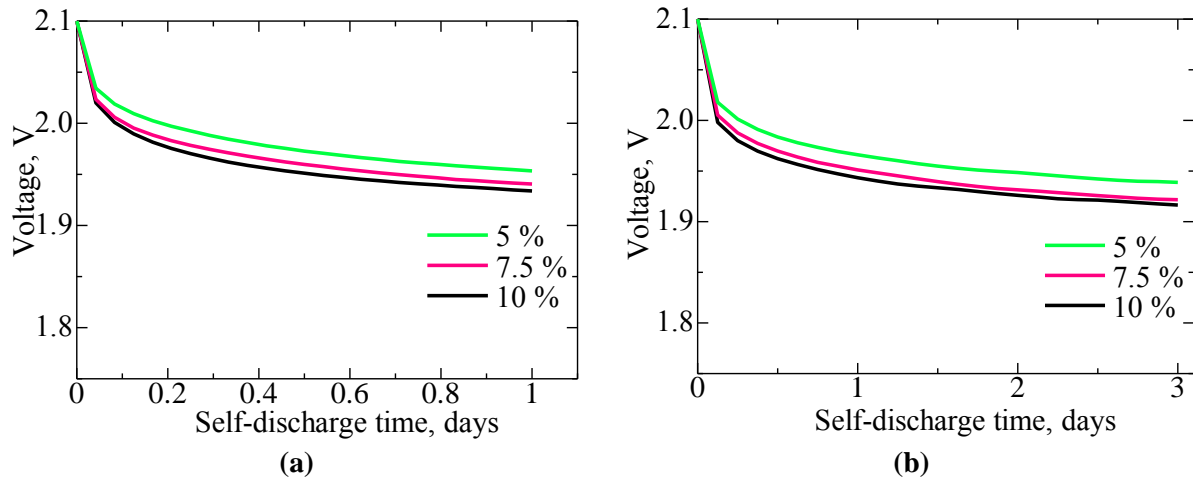


Figure 4. 4 Voltage drop plateau of (a) 1 day and (b) 3 days of OCV for different amount of carbons

Table 4. 1 Summary of voltage drop and remained capacity after days of OCV for different amount carbons

| | 80:10:10 | | 85:7.5:7.5 | | 90:5:5 | |
|---------------|--------------------|---------------------|--------------------|---------------------|--------------------|---------------------|
| | Voltage (V) | Capacity (%) | Voltage (V) | Capacity (%) | Voltage (V) | Capacity (%) |
| 1day | 1.93(8%) | 91 | 1.94(7.6%) | 92 | 1.95(7%) | 93 |
| 3days | 1.92(8.7%) | 84 | 1.92(8.5%) | 86 | 1.94(7.7%) | 89 |
| 15days | 1.89(10%) | 53 | 1.90(9.4%) | 68 | 1.91(9%) | 71 |

4.3.2 Type of Carbon

In order to evaluate the effect of the surface area of the conductive agent, three different carbonaceous materials were selected (see Table 4. 2). As seen in Figure 4. 5 Voltage drop plateau of (a) 1 day, (b) 3 days of OCV and (c) float charge current profile, (d) capacity lost over time for different carbons (a) and (b), the higher the surface area of the conductive additive, the higher the voltage drop of the cells. This is reflected on the self-discharge of the cells after the OCV periods as demonstrated by the bar graph in Figure 4. 5 (c), which shows that KB300 has the worst performance by losing 40% and 45%, after 1 and 3 days of OCV respectively. The float charge current test, accomplished by maintaining the charged cells at

2.1 V for 1 day and observing the current drop (Figure 4. 5 (d)), shows that the KS6 has the lowest current density and KB300 the highest, indicating occurrence of more side reactions when carbon of higher surface area is used.⁷⁹ Hence, it can be inferred that high surface area conductive additives tend to promote the occurrence of side reactions that lead to the cell self-discharge.

Table 4. 2 BET surface areas of different of carbonaceous materials

| Carbon | BET surface area (m ² /g) |
|--------|--------------------------------------|
| KS6 | 17.7986 |
| SP-Li | 60.3388 |
| KB300 | 785.7095 |

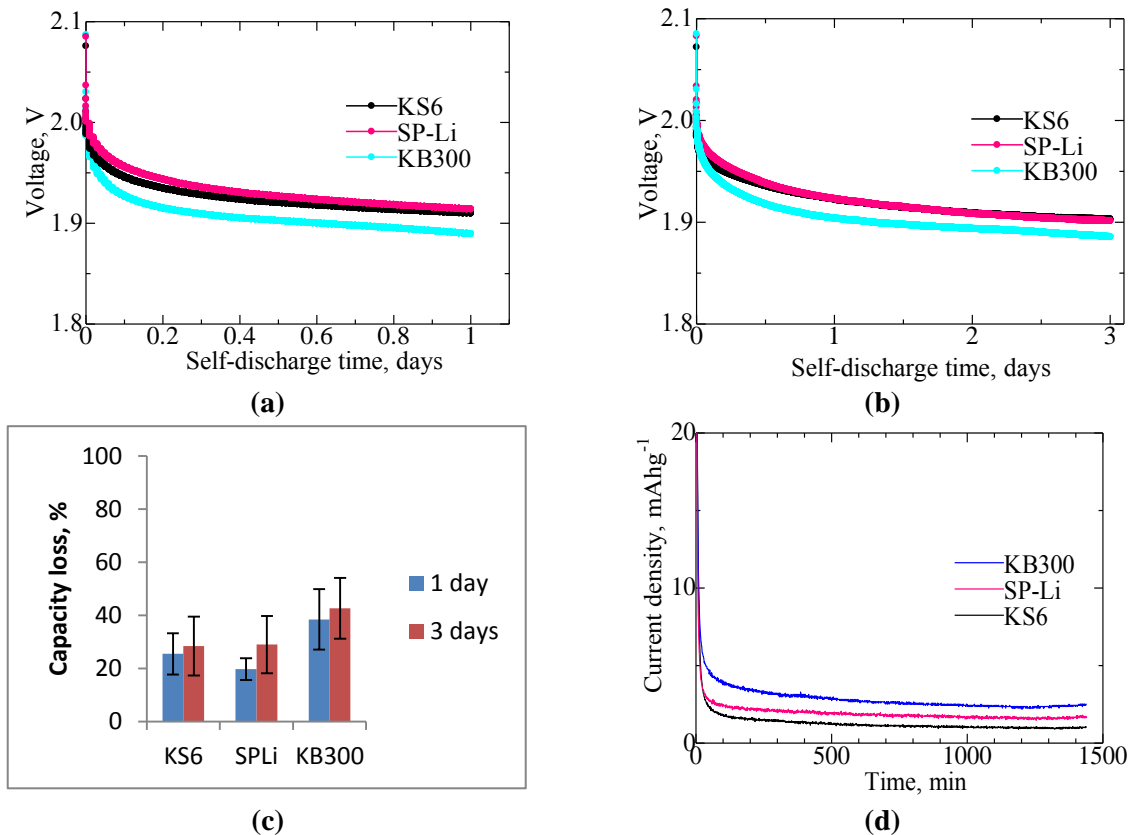


Figure 4. 5 Voltage drop plateau of (a) 1 day, (b) 3 days of OCV and (c) float charge current profile, (d) capacity lost over time for different carbons

AC impedance spectra of electrodes with different carbons (Figure 4. 6) were taken before cycling the cell after charge, after 1 day of OCV, and after discharge (see full experiment description in section 3.3, on page 33), corroborate the aforementioned results. The spectra of the cathodes are similar for the fresh and fully charged cells. After the OCV period (Figure 4. 6 (c)), the cells with carbon of lowest surface areas show the lowest charge transfer resistance.

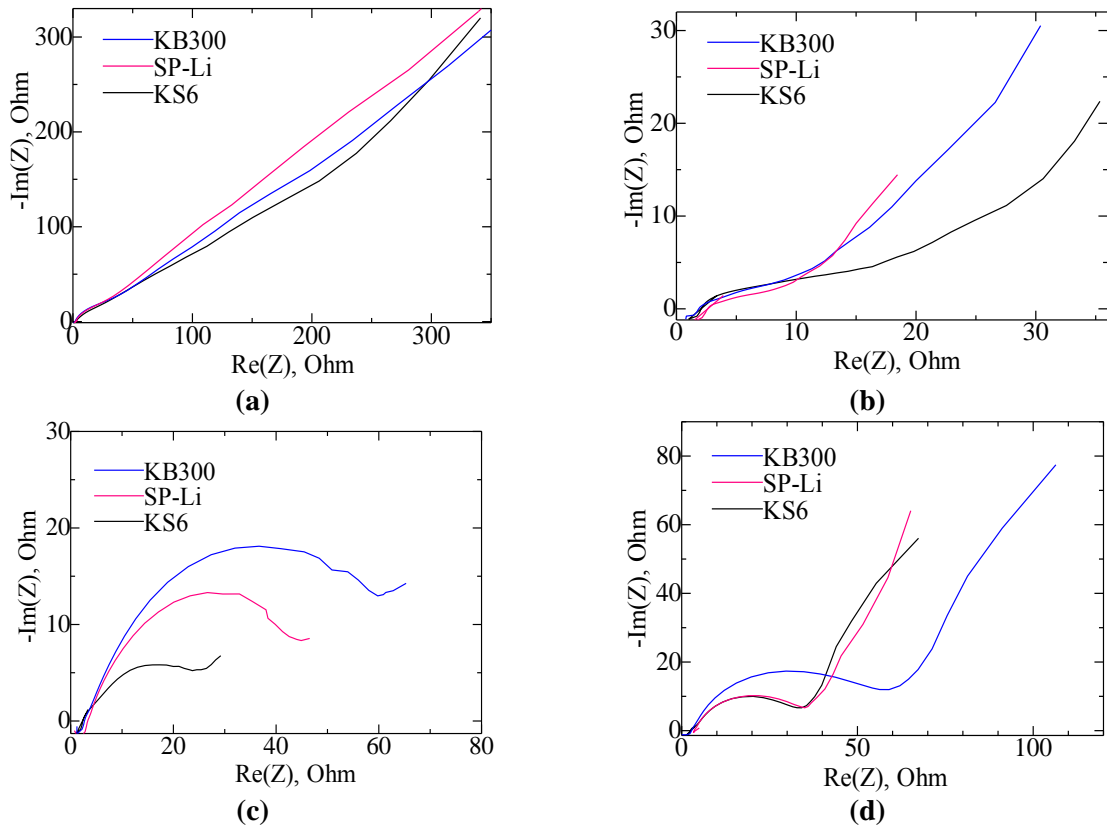


Figure 4. 6 EIS profile of ReHAB cathodes with different carbons: (a) fresh cell; (b) after charge; (c) after OCV for 1 day; d) after discharge.

For sake of comparison, the EIS data for the cells containing Super P-Li as the conductivity enhancer at different stages of charge and self-discharge are plotted together in

Figure 4. 7. The results show that the resistance of the self-discharged cell indeed rests in between that of the discharged and charged states.

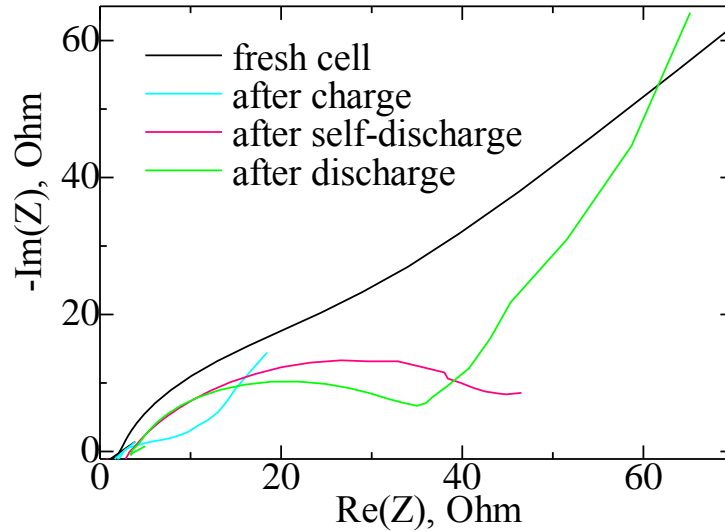


Figure 4. 7 EIS profiles of ReHAB cathode with Super P-Li.

4.4 Effect of different state of charge

The effect of the state of charge (SOC) on the self-discharge characteristics of ReHAB cells was investigated. From previous experiments, it was known that the batteries should not be fully charged due to the fact that, at full charge, ReHAB cells with LiMn_2O_4 cathode can display significant oxygen evolution as a result of hydrolysis of the aqueous electrolyte. Hence, by incompletely charging the cells, self-discharge due to the hydrolysis side-reaction is minimized. This can be achieved by charging the cells to only 2 V, and this strategy does not compromise much of the cell energy density. From the results summarized in Table 4. 3, it can be inferred that the voltage drop and loss of capacity can be minimized by keeping the cells at lower SOC. This suggests that the driving force for the self-discharge

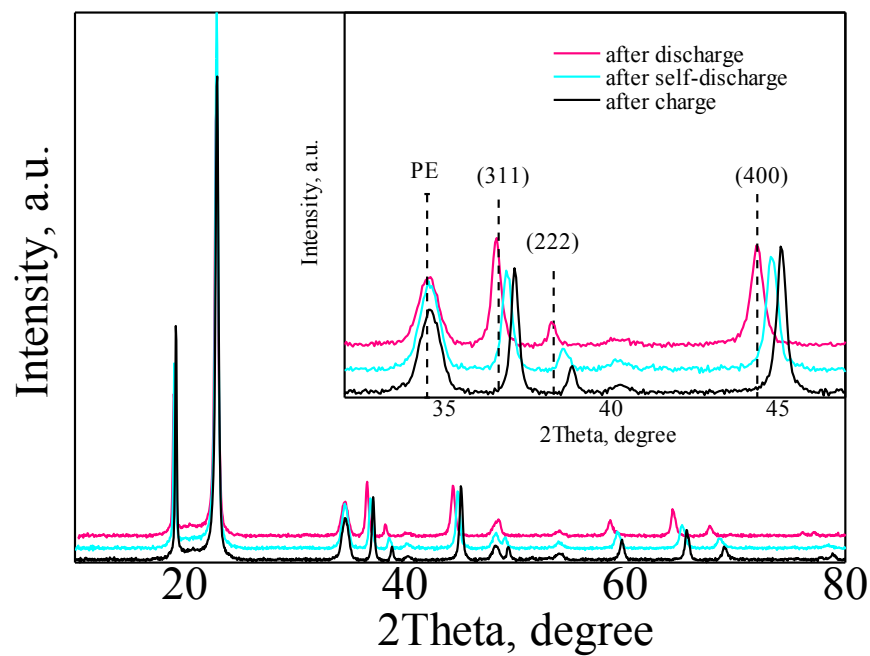
is higher for larger differences of chemical potential of Li, *i.e.* larger difference in composition of the charged state ($\text{Li}_{1-x}\text{Mn}_2\text{O}_4$) to the fully discharged state (LiMn_2O_4). Hence, at least part of the self-discharge process seems to be directly related to the Li^+ intercalation/de-intercalation into/from the active material. To further investigate this supposition, x-ray diffraction of cycled cathodes was performed.

Table 4. 3 Summary of voltage drop and capacity retention of ReHAB cells after 1 day at OCV at the different SOC

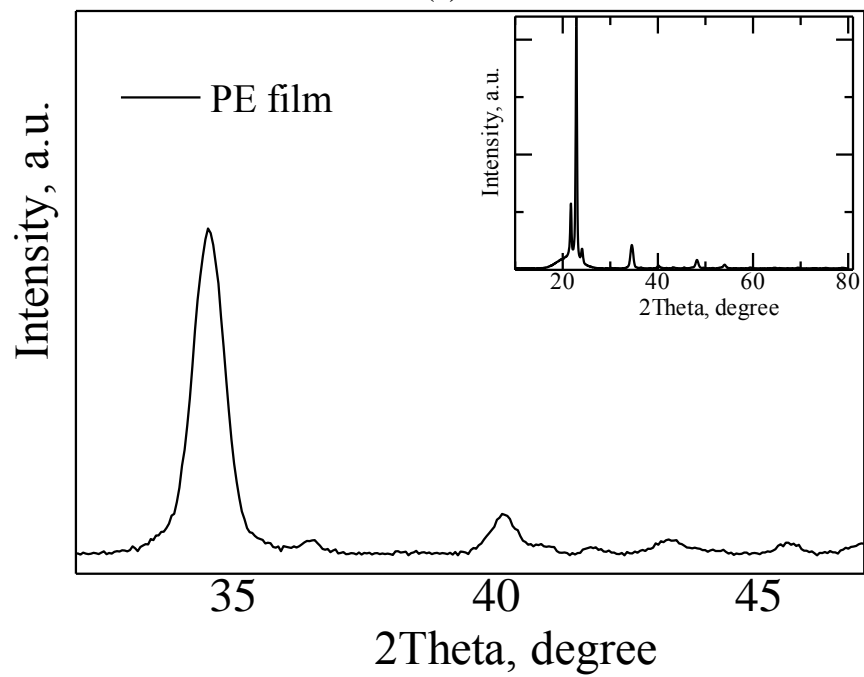
| Initial Voltage | 2.1V | | 2.05V | | 2.0V | |
|------------------------|--------------------|---------------------|--------------------|---------------------|--------------------|---------------------|
| Variable | Voltage (V) | Capacity (%) | Voltage (V) | Capacity (%) | Voltage (V) | Capacity (%) |
| Value | 1.93(8.2%) | 90 | 1.93(5.7%) | 93 | 1.93(3.3%) | 96 |

4.5 *Ex-situ* X-ray Diffraction Studies of ReHAB

Ex-situ x-ray diffraction (XRD) analysis was performed on the cathodes of cells disassembled after one day of self-discharge, and after charge and discharge at constant current (Figure 4. 8). The results show that the lines of the (311), (222), and (400) planes of LiMn_2O_4 of the self-discharged cells shift towards lower diffraction angles, thus indicating lithium re-intercalation into the spinel framework, which results in an increase in lattice parameter.⁸⁴ The line at 34.5° , of the PE current collector, does not change with state of charge of the cells.



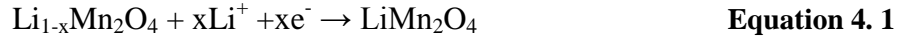
(a)



(b)

Figure 4. 8 XRD profile of (a) after discharged, self-discharged and charged cell and (b) PE current collector

These results denote that at least part of the self-discharge is due to Li^+ re-intercalation into LiMn_2O_4 , according to the following reaction:



To further confirm this assumption, a cell was discharged at very low equivalent rate (0.01C) until the 1.925 V (voltage reached by cells on OCV for 1 day) was reached. This was done to simulate the slow self-discharge process under controlled current. As seen in Figure 4. 9 (a), the voltage profiles of the two cells do not overlap, although the trends are similar. The difference reflects the fact the rate used for the constant current experiment was higher than the rate of self-discharge. Nevertheless, the capacity lost after self-discharge is close to the capacity lost when discharging at low rate (6% and 9%, respectively). Additionally, as depicted in Figure 4. 9 (b), *ex-situ* XRD analysis reveals no significant difference between the diffractograms of the two electrodes.

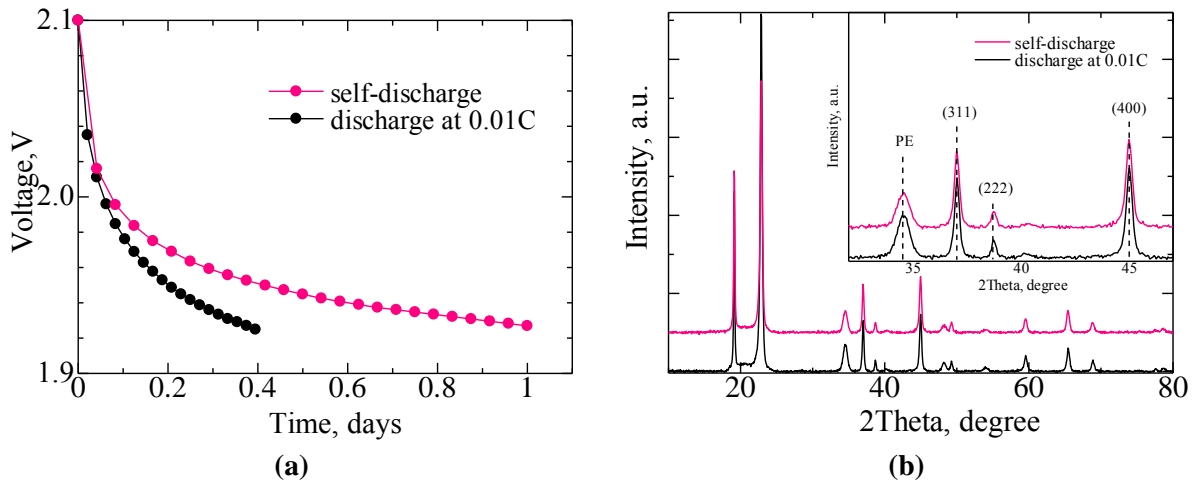


Figure 4. 9 (a) Voltage drop profile and (b) XRD pattern of self-discharged cell and cell discharged at low rate

In addition to the aforesaid data, inspection of the cells capacity after OCV periods indicate that the self-discharge process is largely due to a reversible mechanism, since almost full initial capacity is recovered after 15 days of OCV (Figure 4. 10).

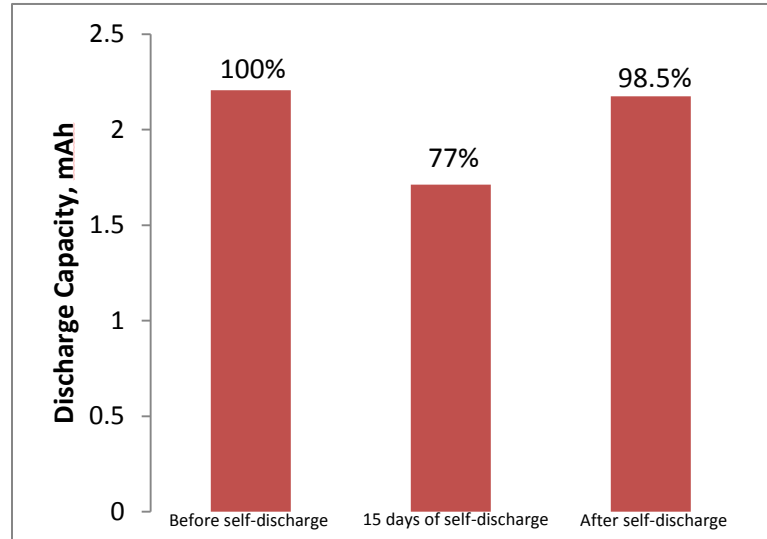
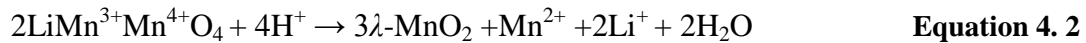


Figure 4. 10 Discharge capacity vs cycle number

These results support the hypothesis that re-intercalation of the Li ions into the cathode material occurs during self-discharge. The lithium re-intercalation could be caused by Zn dissolution back to electrolyte, forcing the Li^+ out of the solution. Guerfi *et. al* showed that dissolution of zinc anode caused high self-discharge in battery systems that use organic electrolyte and polyaniline as cathode.¹⁰³ The authors showed that replacement of the zinc anode with lithium led to better stability of the cells. In the case of the ReHAB system, in which two ions replace each other in the electrolyte during charge/discharge, zinc dissolution pushes lithium back to the cathode.

4.6 Stability of LiMn₂O₄ in the electrolyte

In addition to the reactions discussed in the previous sections, decomposition of LiMn₂O₄ in the electrolyte could also be interpreted as self-discharge. However, this type of reaction would cause loss of active material and would be responsible for the small irreversible loss of capacity observed. The stability of the spinel active material in the electrolyte was evaluated by comparing the XRD pattern of the fresh material with the powder obtained after immersion in the electrolyte solution at 60 °C for one week. Figure 4.11 shows a decrease in intensity of the lines of LiMn₂O₄, indicating reduction of crystallinity of the material. This may be caused by the dissolution of the LiMn₂O₄ into the electrolyte. According to Hunter's reaction, LiMn₂O₄ is not stable in an acidic medium undergoing the following decomposition:⁵¹



Since the incorporated electrolyte was acidic, the above reaction could take place. The XRD pattern of LiMn₂O₄ treated with an electrolyte shows a new line at $2\theta \sim 45^\circ$, likely due to MnO₂.⁵¹ To circumvent this problem, many researchers have tried to coat the surface of the LiMn₂O₄ particles with inactive metal oxides (e.g. ZnO).

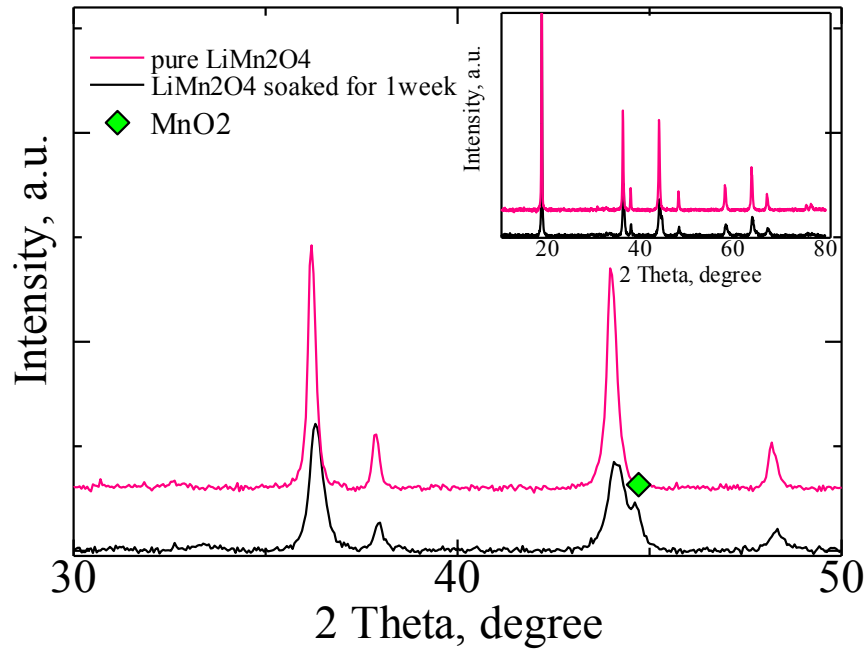


Figure 4. 11 XRD profile of pure LiMn_2O_4 and soaked LiMn_2O_4 for a week

It is important to notice that this experiment was implemented at an elevated temperature, which accelerates the rate of reactions. Although the same results were not observed in the time-frame of the OCV tests, these irreversible reactions could occur at a slower rate, but because the amount of by-products formed was small, they could not be detected in the battery electrodes. This is further confirmed by float charge current tests of ReHAB cells at different temperature. Figure 4. 12 show that at higher temperatures the current density is higher, indicating higher rates of reaction, as per Arrhenius equation.

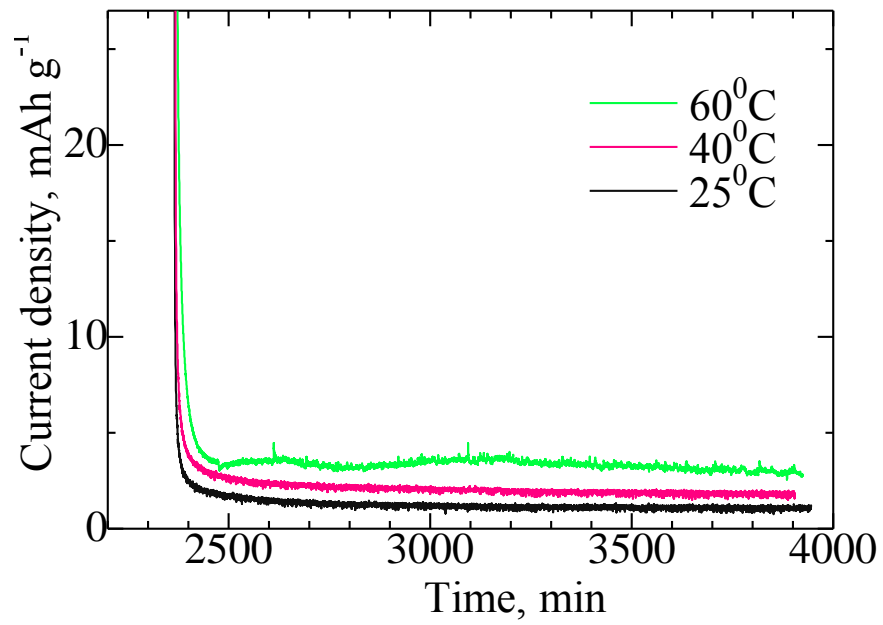


Figure 4. 12 Float charge current profile at different temperature

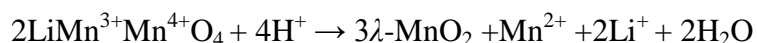
Chapter 5 Conclusions and Future Work

5.1 Conclusions

The effect of different components of the cathode on the self-discharge properties of the new ReHAB system has been studied. A series of electrochemical experiments and supporting *ex-situ* analysis shed important light on the mechanisms responsible for reversible and irreversible capacity loss of the ReHAB cell. The following summarizes the main conclusions:

- The type of current collector being used plays a significant role on self-discharge. Corrosion of the current collector foils is the reaction responsible for this effect, due to Fe ions shuffling into the electrolyte and acting as a reaction catalyst during the open circuit voltage time. Of the three different current collectors studied, conductive polyethylene shows the best resistance to corrosion, followed by graphite and stainless-steel.
- High amounts of conductive agents promote more self-discharge side-reactions. As shown by BET analysis, float charge current tests, and EIS data, the high surface area of the carbonaceous materials are responsible for this effect. Thus, lower amounts of conductivity enhancers of low surface areas reduce the self-discharge of the cells.

- At full charge, the cells are very active and are less stable towards self-discharge. In addition, oxygen generation due to electrolyte hydrolysis is augmented at full charge. Hence, by reducing the state of charge, these problems can be minimized.
- *Ex-situ* XRD analysis of fresh and cycled ReHAB active material indicate that Li re-intercalation back into the cathode is responsible for reversible self-discharge of the cells. This is likely driven by Zn dissolution into the electrolyte.
- XRD analysis revealed instability of the cathode materials in the acidic electrolyte, which appears to cause irreversible loss of capacity during OCV periods, due to decomposition of LMO according to the reaction:



5.2 Future Work

The results presented in this thesis represent the first step in understanding the self-discharge process in the new ReHAB system. Although of paramount importance to develop this technology, with direct impact on the advance of commercialization efforts, it is by no means conclusive. On the contrary, this thesis raises issues that should be addressed in the future, such as:

1. What is the impact of the self-discharge reactions on the storage life of the ReHAB cells?

2. Would surface coated LiMn_2O_4 display better self-discharge performance than the commercial material used in this thesis? What would the best coating material and conditions be?
3. Can the Zn anode be effectively substituted by an alternative Zn^{2+} intercalating material, such as activated carbon? If so, would the system have good electrochemical and self-discharge properties?
4. The results suggested that surface area of the conductive additives plays an important role on the self-discharge. Therefore, the effect of the cathode active material, surface area, and particle size - LiMn_2O_4 and others - on the self-discharge properties of the ReHAB system must also be evaluated.

Bibliography

- (1) <http://www.roskill.com/media/Roskill%20LSM10.pdf/?searchterm=batteries>, R. B. Las Vegas, USA, 2010.
- (2) Tobishima, S.-i.; Yamaki, J.-i. *Journal of Power Sources* **1999**, 81-82, 882.
- (3) Balakrishnan, P. G.; Ramesh, R.; Prem Kumar, T. *Journal of Power Sources* **2006**, 155, 401.
- (4) Li, W.; Dahn, J. R.; Wainwright, D. S. *Science* **1994**, 264, 1115.
- (5) Wang, G.; Fu, L.; Zhao, N.; Yang, L.; Wu, Y.; Wu, H. *Angewandte Chemie International Edition* **2007**, 46, 295.
- (6) Wang, G. J.; Yang, L. C.; Qu, Q. T.; Wang, B.; Wu, Y. P.; Holze, R. *Journal of Solid State Electrochemistry* **2009**, 14, 865.
- (7) Wang, G. J.; Zhao, N. H.; Yang, L. C.; Wu, Y. P.; Wu, H. Q.; Holze, R. *Electrochimica Acta* **2007**, 52, 4911.
- (8) Wang, G. X.; Zhong, S.; Bradhurst, D. H.; Dou, S. X.; Liu, H. K. *Journal of Power Sources* **1998**, 74, 198.
- (9) Wang, X.; Hou, Y.; Zhu, Y.; Wu, Y.; Holze, R. *Scientific Reports* **2013**, 3.
- (10) Wang, Y.; Zhou, H. *Electrochemistry Communications* **2009**, 11, 1834.
- (11) Xu, C.; Li, B.; Du, H.; Kang, F. *Angewandte Chemie International Edition* **2012**, 51, 933.
- (12) Zhang, H.; Wu, X.; Yang, T.; Liang, S.; Yang, X. *Chemical Communications* **2013**, 49, 9977.
- (13) Zhang, M.; Dahn, J. R. *Journal of Electrochemical Society* **1996**, 143, 2730.
- (14) Zhang, S. S. *Journal of Power Sources* **2006**, 162, 1379.
- (15) Yan, J.; Wang, J.; Liu, H.; Bakenov, Z.; Gosselink, D.; Chen, P. *Journal of Power Sources* **2012**, 216, 222.
- (16) Díaz-González, F.; Sumper, A.; Gomis-Bellmunt, O.; Villafáfila-Robles, R. *Renewable and Sustainable Energy Reviews* **2012**, 16, 2154.

- (17) Thackeray, M. M.; Wolverton, C.; Isaacs, E. D. *Energy & Environmental Science* **2012**, *5*, 7854.
- (18) Martin, W.; Ralph, J. B. *Chemical Reviews* **2004**, *104*, 4245.
- (19) Armand, M.; Tarascon, J. M. *Nature* **2008**, *451*, 652.
- (20) Fergus, J. W. *Journal of Power Sources* **2010**, *195*, 939.
- (21) Tarascon, J. M.; Armand, M. *Nature* **2001**, *414*, 359.
- (22) Yoshino, A. *Angewandte Chemie International Edition* **2012**, *51*, 5798.
- (23) Wakihara, M.; Yamamoto, O.; Wiley-VCH: 1998.
- (24) Goodenough, J. B. *Journal of Solid State Electrochemistry* **2012**, *16*, 2019.
- (25) Poizot, P.; Laruelle, S.; Grugeon, S.; Dupont, L.; Tarascon, J. M. *Nature* **2000**, *407*, 496.
- (26) <http://www.rockwoodspecialties.com/> Monika, E.-B. 2008.
- (27) Doughty, D. H. In *Linden's handbook of batteries*; McGraw-Hill: 2011.
- (28) Yazami, R.; Touzain, P. *Journal of Power Sources* **1983**, *9*, 365.
- (29) Ohzuku, T.; Brodd, R. J. *Journal of Power Sources* **2007**, *174*, 449.
- (30) Bazito, F. F. C.; Torresi, R. M. *Journal of Brazilian Chemical Society* **2006**, *17*, 627.
- (31) Mizushima, K.; Jones, P. C.; Wiseman, P. J.; Goodenough, J. B. *Materials Research Bulletin* **1980**, *15*, 783.
- (32) Sun, Y.-K.; Chen, Z.; Noh, H.-J.; Lee, D.-J.; Jung, H.-G.; Ren, Y.; Wang, S.; Yoon, C. S.; Myung, S.-T.; Amine, K. *Nature Materials* **2012**, *1*.
- (33) Gummow, R. J.; Kock, A. d.; Tackeray, M. M. *Solid State Ionics* **1994**, *69*, 59.
- (34) Ohzuku, T.; Makimura, Y. *Chemistry Letters* **2001**, 642.
- (35) Brandt, K. *Solid State Ionics* **1994**, *69*, 173.
- (36) Whittingham, M. S. *Chemical Reviews* **2004**, *104*, 4271.

- (37) Yuan, Y. F.; Wu, H. M.; Guo, S. Y.; Wu, J. B.; Yang, J. L.; Wang, X. L.; Tu, J. P. *Applied Surface Science* **2008**, *255*, 2225.
- (38) Ji, M.-J.; Kim, E.-K.; Ahn, Y.-T.; Choi, B.-H. *Journal of the Korean Ceramic Society* **2010**, *47*, 633.
- (39) Sadeghi, B.; Sarraf-Mamoory, R.; Shahverdi, H. R. *Journal of Nanomaterials* **2012**, *2012*, 1.
- (40) Liu, D.; He, Z.; Liu, X. *Materials Letters* **2007**, *61*, 4703.
- (41) Markovsky, B.; Kovacheva, D.; Talyosef, Y.; Gorova, M.; Grinblat, J.; Aurbach, D. *Electrochemical and Solid-State Letters* **2006**, *9*, A449.
- (42) West, N.; Ozoemena, K. I.; Ikpo, C. O.; Baker, P. G. L.; Iwuoha, E. I. *Electrochimica Acta* **2013**, *101*, 86.
- (43) Tu, J.; Zhao, X. B.; Cao, G. S.; Tu, J. P.; Zhu, T. J. *Materials Letters* **2006**, *60*, 3251.
- (44) Yi, T.-F.; Zhu, Y.-R.; Zhu, X.-D.; Shu, J.; Yue, C.-B.; Zhou, A.-N. *Ionics* **2009**, *15*, 779.
- (45) Shi, J.-Y.; Yi, C.-W.; Liang, L.; Kim, K. *Bulletin of the Korean Chemical Society* **2010**, *31*, 309.
- (46) Gnanaraj, J. S.; Pol, V. G.; Gedanken, A.; Aurbach, D. *Electrochemistry Communications* **2003**, *5*, 940.
- (47) Lim, S.; Cho, J. *Chemical Communications* **2008**, 4472.
- (48) Wu, H. M.; Belharouak, I.; Abouimrane, A.; Sun, Y. K.; Amine, K. *Journal of Power Sources* **2010**, *195*, 2909.
- (49) Liu, H.; Cheng, C.; Hu, Z.; Zhang, K. *Journal of Materials Science* **2005**, *40*, 5767.
- (50) Chan, H.-W.; Duh, J.-G.; Sheen, S.-R. *Surface and Coatings Technology* **2004**, *188-189*, 116.
- (51) Tu, J.; Zhao, X. B.; Xie, J.; Cao, G. S.; Zhuang, D. G.; Zhu, T. J.; Tu, J. P. *Journal of Alloys and Compounds* **2007**, *432*, 313.
- (52) Thackeray, M. *Nature Materials* **2002**, *1*, 81.

- (53) Padhi, A. K.; Nanjundaswamy, K. S.; Goodenough, J. B. *Journal of Electrochemical Society* **1997**, *144*, 1188.
- (54) Ellis, B. L.; Lee, K. T.; Nazar, L. F. *Chemistry of Materials* **2010**, *22*, 691.
- (55) Oickle, A. M.; Andreas, H. A. *The Journal of Physical Chemistry C* **2011**, *115*, 4283.
- (56) Wang, Y.; Yi, J.; Xia, Y. *Advanced Energy Materials* **2012**, *2*, 830.
- (57) Beck, F.; Ruetschi, P. *Electrochimica Acta* **2000**, *45*, 2467.
- (58) Hwang, B.-J.; Tsai, Y.-W.; Santhanam, R.; Hu, S.-K.; Sheu, H.-S. *Journal of Power Sources* **2003**, *119-121*, 727.
- (59) Kandhasamy, S.; Pandey, A.; Minakshi, M. *Electrochimica Acta* **2012**, *60*, 170.
- (60) Lu, Y.; Goodenough, J. B.; Kim, Y. *Journal of the American Chemical Society* **2011**, *133*, 5756.
- (61) Luo, J.-Y.; Cui, W.-J.; He, P.; Xia, Y.-Y. *Nature Chemistry* **2010**, *1*.
- (62) Nakayama, N.; Nozawa, T.; Iriyama, Y.; Abe, T.; Ogumi, Z.; Kikuchi, K. *Journal of Power Sources* **2007**, *174*, 695.
- (63) Ruffo, R.; Wessells, C.; Huggins, R. A.; Cui, Y. *Electrochemistry Communications* **2009**, *11*, 247.
- (64) Tian, L.; Yuan, A. *Journal of Power Sources* **2009**, *192*, 693.
- (65) Minakshi, M. *Electrochimica Acta* **2010**, *55*, 9174.
- (66) Minakshi, M. *Materials Science and Engineering: B* **2012**, *177*, 1788.
- (67) Minakshi, M.; Singh, P.; Sharma, N.; Blackford, M.; Ionescu, M. *Industrial & Engineering Chemistry Research* **2011**, *50*, 1899.
- (68) Minakshi, M.; Kandhasamy, S.; Meyrick, D. *Journal of Alloys and Compounds* **2012**, *544*, 62.
- (69) Minakshi, M.; Singh, P.; Thurgate, S.; Prince, K. *Electrochemical and Solid-State Letters* **2006**, *9*, A471.

- (70) Minakshi, M. *Industrial & Engineering Chemistry Research* **2011**, *50*, 8792.
- (71) Minakshi, M.; Appadoo, D.; Martin, D. E. *Electrochemical and Solid-State Letters* **2010**, *13*, A77.
- (72) Minakshi, M.; Blackford, M.; Ionescu, M. *Journal of Alloys and Compounds* **2011**, *509*, 5974.
- (73) Minakshi, M.; Pritam, S.; Issa, T. B.; Thurgate, S.; De Marco, R. *Journal of Power Sources* **2004**, *130*, 254.
- (74) Minakshi, M.; Singh, P. *Journal of Solid State Electrochemistry* **2011**, *16*, 1487.
- (75) Minakshi, M.; Singh, P.; Issa, T. B.; Thurgate, S.; De Marco, R. *Journal of Power Sources* **2006**, *153*, 165.
- (76) Minakshi, M.; Singh, P.; Issa, T. B.; Thurgate, S.; Marco, R. D. *Journal of Power Sources* **2004**, *138*, 319.
- (77) http://batteryuniversity.com/learn/article/elevating_self_discharge.
- (78) Wang, Z.; Dupré, N.; Gaillot, A.-C.; Lestriez, B.; Martin, J.-F.; Daniel, L.; Patoux, S.; Guyomard, D. *Electrochimica Acta* **2012**, *62*, 77.
- (79) Utsunomiya, T.; Hatozaki, O.; Yoshimoto, N.; Egashira, M.; Morita, M. *Journal of Power Sources* **2011**, *196*, 8675.
- (80) Choi, S. H.; Kim, J.; Yoon, Y. S. *Journal of Power Sources* **2004**, *138*, 283.
- (81) Wang, C.; Zhang, X.-w.; Appleby, A. J.; Chen, X.; Little, F. E. *Journal of Power Sources* **2002**, *112*, 98.
- (82) Yazami, R.; Ozawa, Y. *Journal of Power Sources* **2006**, *153*, 251.
- (83) Aurbach, D.; Talyosef, Y.; Markovsky, B.; Markevich, E.; Zinigrad, E.; Asraf, L.; Gnanaraj, J. S.; Kim, H.-J. *Electrochimica Acta* **2004**, *50*, 247.
- (84) Tarnopolskiy, V.; Kalhoff, J.; Nádherná, M.; Bresser, D.; Picard, L.; Fabre, F.; Rey, M.; Passerini, S. *Journal of Power Sources* **2013**, *236*, 39.
- (85) Utsunomiya, T.; Hatozaki, O.; Yoshimoto, N.; Egashira, M.; Morita, M. *Journal of Power Sources* **2011**, *196* 8598.

- (86) Hosseini Benhangi, P.; Nakhaie, D.; Moayed, M. H.; Molazemi, A. *Journal of Power Sources* **2011**, *196*, 10424.
- (87) Ruetschi, P. *Journal of Power Sources* **2004**, *127*, 33.
- (88) Guo, Y.; Hu, J.; Huang, M. *Journal of Power Sources* **2006**, *158*, 991.
- (89) Gell, R. *A study of lead acid battery self-discharge characteristics*, GELCOservices Pty.Ltd., 2013.
- (90) Wenzl, H. Batteries, Self-discharge. [Online Early Access]. Published Online: 2009.
- (91) B.W. Ricketts; C. Ton-That *Journal of Power Sources* **2000**, *89*, 64.
- (92) Andreas, H. A.; Lussier, K.; Oickle, A. M. *Journal of Power Sources* **2009**, *187*, 275.
- (93) Black, J.; Andreas, H. A. *Electrochimica Acta* **2009**, *54*, 3568.
- (94) *Introduction to Material Science for Engineers*; Shackelford, J. F., Ed.; Pearson International Edition: New Jersey, 2009; Vol. Seventh Edition.
- (95) Koh, K.; Wong-Foy, A. G.; Matzger, A. J. *Journal of American Chemical Society* **2009**, *131*, 4184.
- (96) Sing, K. S. W.; Everett, D. H.; Haul, R. A. W.; Moscou, L.; Pierotti, R. A.; Rouquerol, J.; Siemieniewska, T. *Pure & Applied Chemistry* **1985**, *57*, 603.
- (97) Brunauer, S.; P.H.Emmet; Teller, E. *Adsorption of gases in multimolecular layers* **1938**, *60*, 309.
- (98) www.quantachrome.com, Q. I. P. S. SURFACE AREA DETERMINATION.
- (99) Trunschke, A. *Surface area and pore size determination*, 2007.
- (100) Mancini, M., University of Camerino, 2008.
- (101) Patey, T. J., ETH, 2009.
- (102) Zhang, S.; Ding, M. S.; Jow, T. R. *Journal of Power Sources* **2001**, *102*, 16.
- (103) Guerfi, A.; Trottier, J.; Boyano, I.; De Meatza, I.; Blazquez, J. A.; Brewer, S.; Ryder, K. S.; Vijh, A.; Zaghib, K. *Journal of Power Sources* **2014**, *248*, 1099.